Plasma-enabled synthesis and modification of advanced materials for electrochemical energy storage

Wang, Zhen; Chen, Jian; Sun, Shangqi; Huang, Zhiquan; Zhang, Xiyu; Li, Xiaoying; Dong, Hanshan

DOI:
10.1016/j.ensm.2022.05.018

Document Version
Peer reviewed version

Citation for published version (Harvard):
Wang, Z, Chen, J, Sun, S, Huang, Z, Zhang, X, Li, X & Dong, H 2022, 'Plasma-enabled synthesis and modification of advanced materials for electrochemical energy storage', *Energy Storage Materials*, vol. 50, pp. 161-185. https://doi.org/10.1016/j.ensm.2022.05.018

Plasma-Enabled Synthesis and Modification of Advanced Materials for Electrochemical Energy Storage

Zhen Wang[1], Jian Chen[1,] *, Shangqi Sun[1], Zhiquan Huang[1], Xiyu Zhang[1], Xiaoying Li[2], Hanshan Dong[2,] *

1. Jiangsu Key Laboratory of Advanced Metallic Materials, School of Materials Science and Engineering, Southeast University, Nanjing 211189, China

2. School of Metallurgy and Materials, University of Birmingham, Birmingham B15 2TT

* Corresponding author

E-mail: j.chen@seu.edu.cn, H.DONG.20@bham.ac.uk

Abstract

Plasma, consisting of electrons, ions, molecules, radicals, photons, and other excited species, has not only complex atomic and molecular processes but also versatile physical and chemical reactions with solid materials. This review discusses the contribution of plasma technologies development of electrochemical energy storage systems with emphasis on alkali-ion batteries (lithium-ion batteries, sodium-ion batteries, and potassium-ion batteries), metal-based batteries (*e.g.* zinc metal batteries, lithium metal batteries, and sodium metal batteries), and supercapacitors. A brief overview of the fundamentals and technical effects of plasma technologies and details highlighting the utility of plasma technologies for the synthesis and modification of advanced materials (*e.g.* electrode materials, current collector, and separator) are provided. In this context, the plasma technologies that have been developed for the synthesis and modification of electrode materials with well-defined properties are described, and demonstrations of how these techniques facilitate the regulation of fundamental electrode materials properties as well as the development of new electrode materials are provided. Beyond the discussion of electrode materials, the progress on the current collector and separator are also presented. Finally, the future research directions, challenges, and opportunities of plasma technologies in electrochemical energy storage systems are discussed.

Keywords: Plasma, Synthesis/Modification, Advanced Materials, Electrochemical Energy Storage

1. Introduction

The energy crisis and the environmental pollution have raised the high demanding for sustainable energy sources [1-3]. Although the unlimited natural solar, wind and hydro energies are attractive, their intermittent operation mode requires high-performance energy storage technologies [4]. The advanced electrochemical energy storage (EES) devices, such as alkali-ion batteries, metal-based batteries, and supercapacitors are the most promising solutions, which have been widely investigated. Especially the rational design and synthesis of the advanced materials for electrode materials, current collector and separator are of great importance in developing the superior EES devices.

As the fourth state of a matter apart from solid, liquid and gas, plasma is ionized gas containing equal positive ions and negative electrons, as well as molecules, radicals, photons and other excited species [4]. These active particles possess high momentum and chemical activity and thus interact with materials through a series of physical and chemical effects including diffusion, sputtering and deposition [4]. Although there are various approaches to produce plasma such as combustion, radiation, laser, controlled nuclear reaction and shock [5], the most popular way in laboratory and industry is glow discharge by applying high voltage to two electrodes in a vacuum chamber containing a low-pressure gas, initiating a discharge or ionization between the electrodes. The properties of active particles (*e.g.* proportion, energy) in plasma can be easily controlled by changing processing parameters such as atmosphere, temperature and electrical parameters *etc.*, which realize great capability to modulate the surface properties of materials. Comparing with other methods, plasma technologies have the merits of high efficiency, good controllability, and environmental friendliness. In turn, they have recently emerged as an extremely promising approach for regulating the characteristics of critical materials in electrochemical energy conversion (EEC) and electrochemical energy storage (EES) fields. As has been validated recently by several research reports [4, 6-8], the application of plasma synthesis/modification in EEC have been extensively reviewed, including fuel cells, water splitting, carbon dioxide reduction reaction (CO_2RR), oxygen reduction reaction (ORR), oxygen evolution reaction (OER), electrocatalysts and hydrogen evolution reaction (HER) *etc*. Up to now, several research reports [9-11] had introduced the application of plasma technologies to synthesis/modification electrode materials for EES systems. Furthermore, Joseph *et al*.[12] discussed plasma-enabled modification/synthesis techniques for electrode materials, separators, and electrolytes, but only limited to lithium-ion batteries. In view of the rapid development of the plasma in versatile EES devices as well as various components, a comprehensive and critical state-of-art review is necessary and urgent.

In this review, we devote to highlighting the fundamental mechanisms and technical features of plasma as well as its fruitful applications in EES systems, as shown in **Figure 1**. Firstly, we introduce the plasma fundamentals including the concept, classification, and discharge theories, and particularly focus on the discharge process and modes of widely used non-thermal plasma. Secondly, the plasma-introduced physical and chemical effects are discussed. Based upon, the applications in EES systems are reviewed, and particular concerns have been placed on electrode materials for alkali-ion batteries (lithium-ion batteries, sodium-ion batteries, and potassium-ion batteries), metal-based batteries (*e.g.* zinc metal batteries, lithium metal batteries, and sodium metal batteries), and supercapacitors. Moreover, the use of plasma-based modulation on the current collector and separator are also introduced. Finally, we propose the future research directions, challenges, and opportunities of plasma technologies in EES systems. All in all, we hope that readers can understand the core

knowledge and mechanisms of plasma, realize that plasma-enabled strategy is an interesting and fruitful field, further deepen the understanding of the science and develop targeted plasma technologies, finally promote the applications and the commercialization.

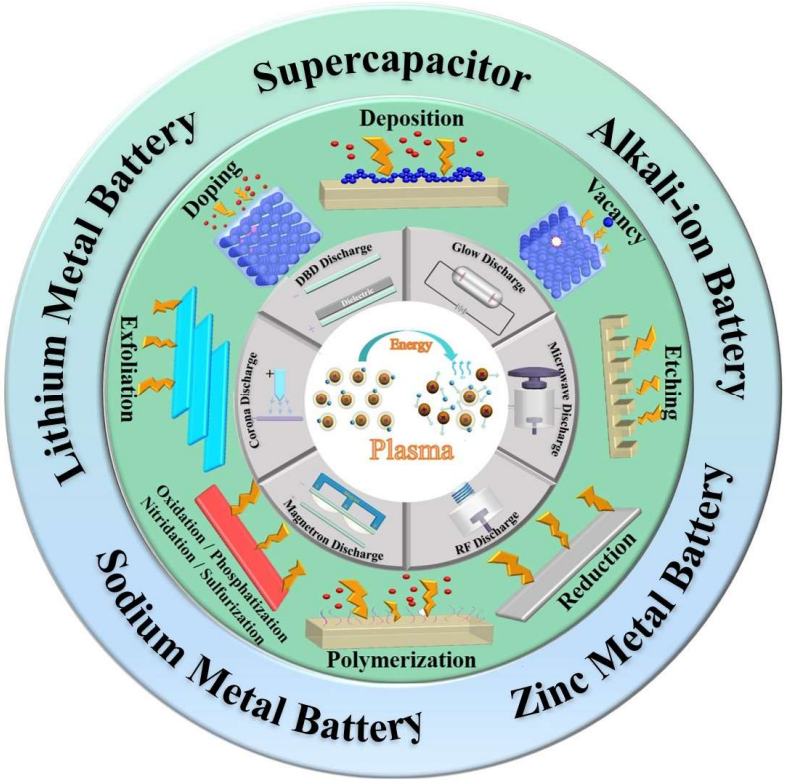

Figure 1. The schematic diagram of plasma, the discharge modes, the plasma-introduced effects, and their applications in electrochemical energy storage systems

2. Fundamentals of Plasma and Plasma Technology

2.1 Brief on Plasma

In 1928, Irving Langmuir first used the "plasma" to describe the region containing balanced charges of ions and electrons [13, 14], meaning that the electron densities (n_e) are approximately equal to the ion densities (n_i). Although the plasma is 'quasi-neutral' [15], the free charge carriers (electron and ion) can not only endow the higher electrical conductivity than metals (*e.g.* copper and gold), but also produce prolific source of excited particles, giving its unique properties against other matter states (solids, liquids and gases). More importantly, plasma has two attractive characteristics for practical applications [16]. Firstly, the particle temperature and energy density in plasma are higher than those in other states. Secondly, plasma can also generate energetic species, even at low temperatures, which can initiate physical and chemical reactions that are difficult or impossible to obtain using other processes.

Since plasma occurs over a wide range of situation, according to electron temperature (T_e, in eV, 1eV equal to ~11600 K) and electron densities (n_e), the plasma can be divided into two categories: natural and man-made, as described in **Table 1**. As we know, naturally occurring plasmas comprise the majority of the visible universe, encompassing the solar corona, solar wind, nebula and the earth ionosphere *etc*. In earth atmosphere, the low temperatures and high pressures are not favorable for the formation of plasma except under unusual conditions. The lightning and Aurora Borealis (or

northern lights) are probably the most common natural plasma phenomenon on earth. The use of electric discharge is one of the most common ways to create and maintain man-made plasma, in which the energy from the electric field is transferred to electrons and heavy particles through a series of collisions. When the T_e and the heavy particle temperature T_h are close to each other, reaching the state of local thermodynamic equilibrium, the plasma is termed thermal plasma. Conversely, when there is large departure from this condition ($T_e >> T_h$), the plasma is termed non-thermal plasma, in which the T_e can reach over 1 eV with heavy particles (ions and neutral particles) temperatures approaching room temperature [16, 17]. This is due to the external electric field can provide more energy to the electrons than the heavier particles, even with a high collision frequency. In comparison with the thermal plasma, although the non-thermal plasma has lower temperature of active particles, it requires less input energy, generates less total neat and hence shows better practicability including flexible controllability, diverse discharge modes and cost effectiveness [18-20]. Non-thermal plasma has been widely used in the versatile fileds including plasma surface engineering [21-23] and hence, it is the focus of the review paper.

Table1 Classification of kinds of plasma [16, 17]

Plasma		State	Electron temperature	Electron densities
Natural		Thermodynamic equilibrium	$T_e \approx 10^2$ eV	$n_e \geq 10^6$ /cm^3
Man-made	Thermal plasma	Local thermodynamic equilibrium	$T_e \approx 1$~20 eV	$n_e \geq 10^{10}$ /cm^3
	Non-thermal plasma	Non thermodynamic equilibrium	$T_e \approx 1$~20 eV	$n_e \geq 10^{10}$ /cm^3

2.2 Discharge processes and modes of non-thermal plasma

(i) Discharge processes

Glow discharge is a widely used way to produce non-thermal plasma, which owes its name to the fact that the plasma is luminous. According to more descriptive physical definition, a glow discharge is the self-sustained continuous directly current (DC) discharge having a cold cathode that emits electrons as a result of secondary emission mostly induced by positive ions [16]. **Figure 2** displays the schematic diagram of discharge processes in a low current, high voltage device where the gas is weakly ionized. When a high potential is applied to two electrodes, discharge, or ionization initiates with the electron-atom collision in gas, which results in the emission of electrons, the ions (electron impact ionization) and the metastable atoms with superscript * (electron impact excitation). Meanwhile, the metastable atoms, which have more energy than their ground states, can produce cumulative ionization to increase the electron density through Penning ionization and metastable ionization, and more metastable atoms (ion impact excitation). The relaxation of metastable atoms generates luminous glow due to the emission of photons with the energy and hence wavelength determined by the atomic structure. Besides these processes, the dissociation of molecules and charge/electron transfers also take place in plasma. In turn, although there is a continuous loss of electrons at the electrodes, there must be an equal degree of ionization going on by ionization, excitation, and dissociation to

maintain the steady state. Additional electrons can be produced by secondary emission from the cathode, which is also important to maintain a sustainable discharge. To be noted, the discharge processes are strongly influenced by the operating parameters (*e.g.* power, gas, pressure and electrode geometry).

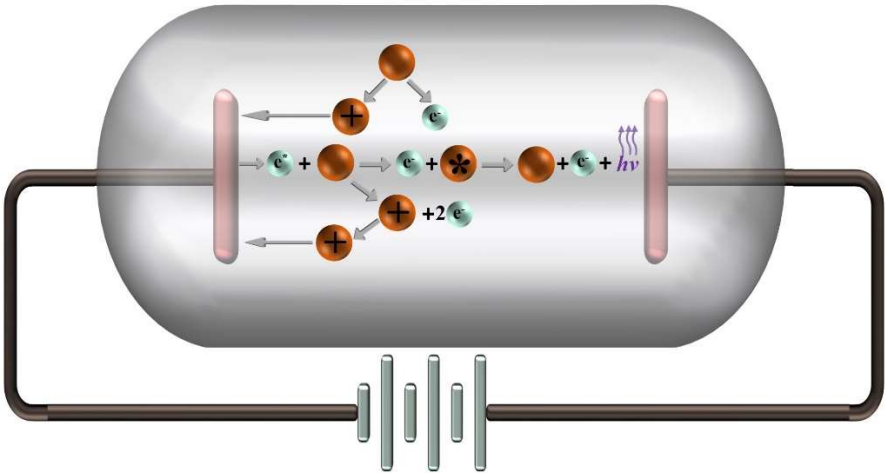

Figure 2. Schematic diagram of glow discharge processes

(ii) Discharge modes

Traditional DC glow discharge is a commonly used with different feedstocks (CH_4, H_2, O_2, N_2, Ar, NH_3, H_2S, PH_3 *etc.* [9, 24, 25]). However, this mode has some technical issues, such as high discharge voltage, high discharge pressure, low ionization degree, low current density, and for conductive electrodes, which limits its use. Thus, some other generation modes have been developed, such as radio frequency (RF) discharge, microwave discharge, magnetron discharge, corona discharge and dielectric barrier discharge (DBD) *etc.*, and the specific discharge diagrams have been shown in **Figure 1**. Meanwhile, the advantages and applications of six plasma technologies are shown in **Table 2**. In addition, several publications [4, 5, 16, 26] have introduced these plasma technologies in details, the readers also can refer them for details.

Table 2. Advantages and applications of various plasma technologies

Mode	Mechanism	Applications	Advantages
Glow discharge	High voltage	Surface processing (*e.g.* etching and doping	Simple, inexpensive, wide pressure range
DBD	High voltage/Frequency (0.05~500kHz)	Synthesis and modification of materials	Simple excitation, wide pressure range, large plasma discharge zone, the flexibility of geometrical configuration and operating medium
Corona discharge	Uneven electric field	Surface modification of polymers	Self-sustaining discharge, relatively low current
RF discharge	Alternating frequency (1kHz~10^3 MHz)	Synthesis of materials, surface processing (*e.g.* cleaning, etching, doping)	Less charge accumulation
Magnetron	Alternating electric/magnetic field	Synthesis of thin films or	High film purity and

discharge		coating	density, controllable film thickness
Microwave discharge	Electromagnetic wave (300MHz~10 GHz)	Synthesis of nanaomaterials	High degrees of ionization and dissociation, highly controllable material preparation

3. Plasma-introduced effects

As mentioned above, the complex discharge processes bring different combinations and states of active species (electron, ions, and neutral particles) in plasma, which can promote versatile physical and chemical reactions with interacted solids. Herein, the plasma-introduced effects as depicted in **Figure 1** are discussed as follows.

3.1 Physical effects

(i) Exfoliation

When the high-energy particles of plasma interact with a material surface by momentum transfer, the activated surface atoms/molecules can overcome weak inter-molecular force, *e.g.* van der Waals force or hydrogen bond. Thus, 2D layered materials including graphene and layered double hydroxides [8, 10] can be exfoliated by plasma. Compared with traditional exfoliation methods, *e.g.* mechanical exfoliation or solvent-assisted exfoliation, plasma exfoliation is more efficient and involves no toxic or environmentally unfriendly chemicals or gases. Moreover, the plasma-exfoliated products are usually free of contamination such as surfactants, maintaining their intrinsic properties.

(ii) Vacancy

During the momentum transfer with the incident active particles in plasma, the surface atoms or ions can be sputtered out to leave vacancies in the lattice, which is opposite to deposition or implantation. The sputtering extent can be modulated by the type, energy, and direction of incident particles. So far, various vacancies including cationic vacancies (*e.g.* Co and Fe vacancies), anionic vacancies (*e.g.* O, S and N vacancies), and multi-vacancies (*e.g.* cationic and O vacancies), have been reported due to their low formation energy [27] as well as attractive effects in modulating materials properties. Compared with many other methods (*e.g.* heat treatment, chemical methods), plasma technology has the advantages of high efficiency, good controllability, and environmental friendliness.

(*iii) Doping*

Doping with non-metal elements (*e.g.* N, O, S, P, B, F, *etc.*), metal elements (Mg, Ti, Fe, Al, Ni, Cu, *etc.*) and dual/triple elements (*e.g.* N-S, N-P, N-S-P) has been widely used in modulation the materials for EES devices [28, 29]. As mentioned before, the momentum transfer can confer high energy to particles in plasma, which can be implanted into the framework of the matrix material, realizing the doping effects. Comparing with the *in-situ* growth [30], plasma doping can make the acceptor doped in a highly activated state with a high efficiency.

(iv) Deposition

Plasma has been widely used to deposit coatings and thin films. Compared to the deposition driven by thermal (*e.g.,* thermal evaporation, thermal chemical vapor deposition), plasma enhanced deposition can greatly lower the nucleation barrier due to the high reactivity of the species, and thus allow for more freedom in selecting processing conditions (*e.g.,* temperature, time, atmosphere, and substrate). Thus, various materials can be deposited by plasma technologies, such as carbon, metals, oxides, and nitrides [10, 31].

(v) Etching

Besides physical sputtering behavior, the excited/charged particles in plasma possess high chemical activity, which promote the chemical reaction (*e.g.* reactive ion etching) to form volatile products. These physical and chemical reactions thus result in surface etching effects. Compared with other technologies (*e.g.* wet chemical etching), plasma etching is highly reproducible and well-controlled. Moreover, etching selectivity and higher etching rate can be achieved by controlling the composition and rate of the discharge gas [32].

3.2 Chemical effects

(i) Oxidation/Nitridation/Sulfurization/Phosphorization

Plasma has been often used to functionalize the materials by oxidation, nitridation, sulfurization and phosphorization to prepare versatile surface compounds, which introduce improved anti-corrosion, enhanced electrical conductivity and electrochemical performances and so on. For example, the oxygen-containing plasma (O-plasma) can produce active oxygen species (O, O^+, O^-), which are prone to reacting with metals to form oxides or peroxides [33]. Similarly, nitrides [34], sulfides [35], phosphides [36] can be formed in nitrogen plasma (N-plasma), sulfur plasma (S-plasma), phosphorus plasma (P-plasma) respectively, using different feedstocks (N_2, NH_3, H_2S, PH_3 *etc*.).

(ii) Reduction

The plasma formed with reducing gas feedstock such as hydrogen (H-plasma) has been widely used to reduce or remove oxides (*e.g.* CuO, graphene oxide [37, 38]) due to the abundant atomic hydrogen, ionic hydrogen, excited hydrogen atoms and hydrogen molecules. Comparing with thermal reduction, the plasma-introduced reduction can take place at a lower temperature with good controllability, broadening the material application, especially for the temperature-sensitive ones. In addition, the plasma method is also attractive due to its environmental benignity and safety.

(iii) Polymerization

During exposure in plasma, monomers can react through addition polymerization or condensation polymerization. The surface properties can be significantly altered by plasma polymerization, such as surface energy, hydrophilicity, and adhesion. Meanwhile, the polymerization process can be controlled by the atmosphere, monomer type, substrate, and processing time, *etc.* However, the mechanisms of plasma polymerization are still subject to debating. Currently there are several proposed mechanisms including radical chain growth polymerization, ionic chain growth polymerization, ion-molecule reactions, monomer fragmentation-poly-recombination, radical chain growth copolymerization, as well as chemical grafting onto radical sites or functional groups [39].

Based upon, the plasma has high reactivity and multiple discharge modes. Comparing with other methods *e.g.* hydrothermal, calcination which rely on harsh reaction conditions (chemicals, high temperature/pressure, long duration), the plasma-based processes are general environmentally friendly, controllable and efficient. More importantly, they can endow materials with novel structures and excellent properties through versatile physical and chemical effects, including exfoliation, deposition, etching, defects (doping/vacancy), surface functionalization and polymerization. Therefore, they have attracted considerable attention in the synthesis and modification of critical materials for science advance and technology innovation in EES fields.

4. Plasma Applications for Electrochemical Energy Storage

This section is devoted to the applications of plasma technologies for various EES devices with an emphasis on electrode materials. As have been discussed in previous sections, advanced plasma technologies can produce a series of desirable functions and hence have two main applications for electrode materials: i) to synthesize nanomaterials or composites on the nanoscale; and ii) to modify the material surface via plasma-introduced effects. Hence, for each type of electrode material, we first introduce some examples of plasma synthesis, followed by some examples of plasma modification. Beyond the discussion of electrode materials, several examples on the modification of current collector and separator by advanced plasma technologies are also introduced.

4.1 Plasma Synthesis and Modification of Electrode Materials

4.1.1 Lithium-Ion Batteries (LIBs)

LIBs have been successfully commercialized and widely used in portable electronic devices (smart phones, computers), electric transportation (electric vehicles) and large energy storage devices (power grid) and so on [40]. However, the ever-increasing demands for high-performance rechargeable batteries (high energy density, fast charging ability and long cycle stability *etc.*) push researchers to look for better electrode materials [41]. So far plasma has been successfully utilized to modify and fabricate the electrode materials for LIBs. This section will review some typical researches on the application of plasma technology for various electrode materials. Meanwhile, the summary of synthesis/modification of electrode materials in LIBs by plasma technologies have also been presented in **Table 3**.

4.1.1.1 Anode materials

Graphite materials are the dominant commercial anode materials. But they suffer from low capacity (372 mA h/g) that limits the energy density of LIBs, and the unsatisfactory diffusion rate of Li^+ that results in low ratability especially at low temperature. In turn, various anode materials have been proposed, and can be divided into three categories based on the storage mechanisms: intercalation reaction-based, alloying reaction-based, and conversion reaction-based materials [42]. The plasma technologies have been applied for synthesis and modification of above-mentioned materials, which will be discussed in the following sections.

(i) Intercalation-based materials

Ti-based materials are frequently reported anode materials for LIBs and most of them exhibit the intercalation reaction-based mechanism. Among the commonly reported Ti-based materials, TiO_2 and $Li_4Ti_5O_{12}$ have received enormous attention. TiO_2 with

different crystal structures (*e.g.* amorphous, anatase, and rutile) are a promising anode materials due to low cost, non-toxicity, environmental friendliness, high working voltage (around 1.7V vs. Li/Li^+) and structural stability during lithium insertion/extraction [43]. Among various polymorphs, anatase TiO_2 has been proved to exhibit the highest electrochemical activity because of its 2D diffusion routes as well as abundant accommodation sites for ions intercalation [44, 45]. Nevertheless, the inherently poor conductivity gives rise to its sluggish reaction kinetics and inferior rate capability. Specifically, some plasma approaches have been reported to improve the electrical conductivity, such as defect engineering (oxygen vacancy, Ti^{3+} ions), nano/micro-structure, nanocomposite and so on, to achieve the higher rate capability and power density. Sun *et al.* [46] recently demonstrated the application of Ar/N_2 plasma to modulate the MOF (metal-organic framework)-derived TiO_2/C nanocomposites as shown in **Figure 3a**. The introduction of defects including oxygen vacancies (OVs), Ti^{3+} ions and lattice distortion in TiO_2 can significantly improve the intrinsic conductivity. Moreover, the specific surface area can be increased by controlling the plasma power without damaging the nano/micro-structure. Therefore, the as-fabricated electrode exhibited much improved electrochemical performance with an ultra-high reversible capacity (316.9 mA h/g at 0.5 A/g), excellent rate capability (186.1 mA h/g at 10 A/g) and long cycle life (219.3 mA h/g after 2500 cycles at 5 A/g). In addition, Li *et al*. [47] reported that the H_2 plasma is a simple and effective way to substantially enhance the electron conductivity and Li^+ mass transport of TiO_2 nanowires by introducing Ti^{3+} ions. As shown in **Figure 3b**, a single plasma-treated TiO_2 nanowire (H-TiO_2) approximately 50 nm in diameter, and high magnification TEM image and SAED pattern further indicate that the H-TiO_2 nanowire is single crystalline grows along the [100] direction. The H-TiO_2 nanowires thus exhibits higher lithium storage capacity and rate capability than the pristine TiO_2 nanowires.

The $Li_4Ti_5O_{12}$ (LTO) has also received much attention as a commercialized anode material for LIBs due to its unique features, such as negligible volume change ("zero-strain" material), excellent structural stability, and a flat Li-ion insertion potential (around 1.55V vs. Li/Li^+) at which the formation of the solid electrolyte interphase (SEI) layer can be avoided [48]. However, LTO is also significantly underappreciated due to the similar problems [49] (low conductivities) as for TiO_2. To overcome these drawbacks, introducing OVs has been proved as an efficient strategy to improve the capacities at high rates due to enhanced bulk capacities and surface capacitance. In an early research [50], the LTO was doped by N^{3-} ions into O^{2-} sites through Ar/N_2 plasma at atmospheric pressure. The introduced OVs and Ti^{3+} as well as the reduced surface particles resulted in the obvious enhancement of Li storage behavior. Moreover, Zhu *et al.* [51] have also successfully introduced OVs into LTO (denoted as PLTO) via an eco-friendly and cost-effective H_2/N_2 plasma process. As shown in **Figure 3c**, the PLTO not only delivered high lithium storage ability (173.4 mA h/g at 1C), but also exhibited impressive rate capacity. The enhanced lithium storage mechanisms especially at high rates are dominated by the insertion behavior and dual-phase conversion because the expanded lattice may facilitate ion diffusion.

Apart from the Ti-based materials, the nitrogen-containing carbon materials have also received widespread attention as the N can increase electrical conductivity. For example, the easy accessibility and low-cost graphitic carbon nitride (g-C_3N_4) corresponds to a high theoretical capacity of 524 mA h/g. However, the large amount of pyridine nitrogen (C-N-C) and graphitic nitrogen (C_3N) in g-C_3N_4 deteriorate the electronic conductivity. Mg-templated de-nitriding has often been used to reduce nitrogen content,

which can introduce nitrogen vacancies (NVs), and expanded interlayer distance. But this method is difficult to be controlled, and the high content NVs are thermodynamically unstable, leading to phase and structure degradation. Herein, Sun *et al.* [52] proposed a heteroatom-refilling strategy of refilling oxygen in plasma-induced highly nitrogen-deficient g-C_3N_4. As shown in **Figure 3d**, through the H_2-plasma bombardment, the highly nitrogen deficient g-C_3N_4 is prepared. To refill oxygen, the nitrogen deficient g-C_3N_4 is exposed in air for more than 24h (denoted as HGCN). Oxygen refilling can not only stabilize the nitrogen-deficient g-C_3N_4 structure, but also boost the conductivity. Meanwhile, the lithium adsorption energy of the refilled oxygen is higher than that of the intact g-C_3N_4. Benefiting from the above advantages, the HGCN displays superior lithium storage performance, including high specific capacity (647 mA h/g after 400 cycles at 0.1 A/g) and remarkable cycle performance (232.8 mA h/g after 5000 cycles at 1 A/g).

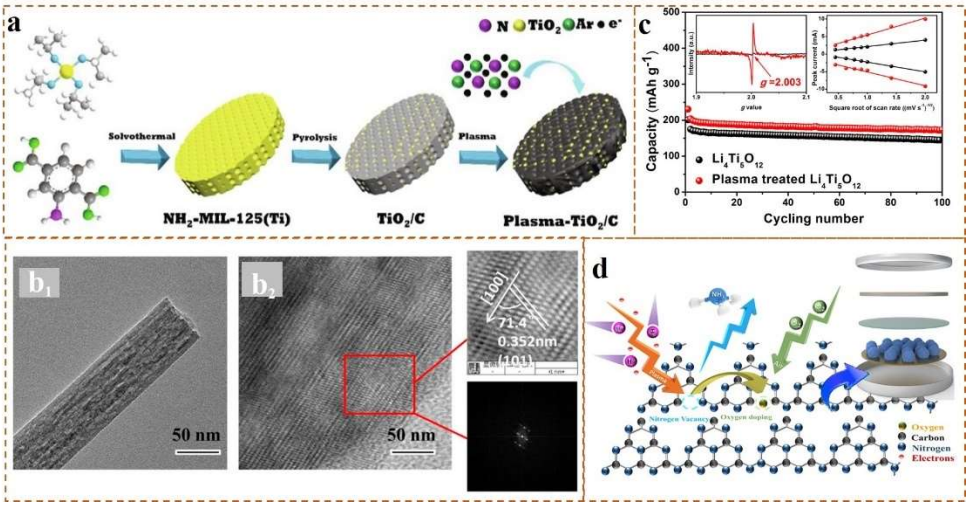

Figure 3. a) Schematic of the preparation procedure of plasma modified TiO_2/C. Reproduced with permission [46], Copyright 2021, Elsevier. b_1) the TEM image a single H-TiO_2 nanowire and b_2) high magnification TEM image and SAED pattern in H-TiO_2 nanowire. Reproduced with permission [47], Copyright 2016, Elsevier. c) cycling performance of LTO and PLTO at 1C. Reproduced with permission [51], Copyright 2019, American Chemical Society. d) the formation mechanism diagram of refilling oxygen in plasma-induced highly nitrogen-deficient g-C_3N_4. Reproduced with permission [52], Copyright 2022, Elsevier.

(ii) Alloying-based materials

Alloying elements (*e.g.* Si and Al) have attracted considerable attention due to their abundance, low price, and high theoretical capacity [53, 54]. For example, the Al can convert to Li rich intermetallic compounds LiAl, Li_3Al_2 and Li_9Al_4 at low equilibrium potential (0.23~0.38) V vs. Li/Li^+, corresponding to a high theoretical capacity of at least 993 mA h/g [55]. However, Al based anode suffers not only large volume change during charge/discharge but also a dense surface inert oxide layer (more severe for small particles) that retards both electron and Li^+ transport [56]. In view of these, Chang *et al.* [57] recently prepared a ultrafine and homogeneous Al-Fe/C nanocomposite using inductively coupled plasma (ICP) with Ar-H_2-CH_4 gas, $AlCl_3$ and $FeCl_3$ at near room temperature in **Figure 4a**. The H species in plasma can reduce the volatile $AlCl_3$ and $FeCl_3$ to form metallic Al and Fe, while the CH_4 acts as the carbon source. The formed Fe not only facilitated the decomposition of CH_4 on the surface of Al nanoparticles to inhibit the growth and aggregation of the Al particles, but also formed compact carbon

coating to suppresses surface oxidation. In turn, the Al-Fe/C sample exhibited high specific capacity of 927 mA h/g after 600 cycles at 100 mA/g, and better electrochemical kinetics and lower charge transfer impedance compared to the Al/C sample.

In addition, the theoretic capacity of Si reaches 4200 mA h/g by the formation of $Li_{4.4}Si$, which is more than 10 times higher than that of graphite [58]. However, the dramatic volume change (~360% for $Li_{4.4}Si$ [59]) and huge stress are concomitant with the alloying process, which has severely handicapped its commercial applications. The fabrication of oxide outer layers (*e.g.* SiO_x [60, 61], TiO_2 [62]) on Si-based materials is a promising strategy. In a recently reported research [63], a simple and green atmospheric plasma oxidation strategy is exploited to fabricate SiO_x layer on the surface of Si nanoparticles, as shown in **Figure 4b**. The SiO_x layer not only effectively reduced the volume change of Si, but also improved the wettability of the electrolyte, thus promoting the Li^+ transmission at the electrode-electrolyte interface. In addition, TiO_2 coating has often been applied to sustain the volume change of alloying-based anode materials due to its mechanical robustness [64, 65]. In order to overcome the low intrinsic conductivity of TiO_2 as-mentioned above, plasma-driven heteroatom doping (such as N, B, and F atoms) has been proved to be an effective way to narrow the band gap and improve the conductivities [66]. For instance, Hu *et al.* [62] compared the performance of SiO_x@Si nanoparticles encapsulated in pure TiO_2 layer (TSO) and N-doped $TiO_{2-\delta}$ layer (N-TSO) by N_2 plasma treatment, as shown in **Figure 4c**. It is found that although both SiO_x and TiO_2 layers act as binary buffer matrices to accommodate the large volume change and stabilize the SEI layer on the shell surface, the plasma-induced N-doped $TiO_{2-\delta}$ layer can not only further improve the electrode stability but also ameliorate the electrical conductivity and interfacial electrochemistry due to the Ti^{3+} species and OVs. Therefore, the N-TSO exhibited better cycling stability with a capacity retention (650 mA h/g over 300 cycles at 200 mA/g) in comparison with TSO.

(iii) Conversion-based materials

Transition metal compound, M_aX_b (M = transition metal, X = O, S, F, N, *etc.*) reacts with Li to form metallic nanoparticles embedded in the Li_nX matrix through conversion reaction, which can be described as $M_aX_b + yLi \leftrightarrow aM + bLi_nX$ [42]. Recently, a tetragonal ε-Ti_2N is stably synthesized by N_2 plasma exposure process via the reaction between α-Ti thin film and nitrogen ions, which is actually the most stable phase of Ti_2N rather than the hexagonal one [67]. As the anode material of LIBs, the cyclic voltammetry (CV) is utilized to reveal the behavior of the conversion reaction between Li^+ and ε-Ti_2N, a reduction peak at ~0.22V possibly originating from the formation of Li_5TiN_3 and/or Li_2TiN_2 between Li^+ and ε-Ti_2N. As the voltage keeps decreasing, the reduction peak at ~0.02 V might result from the formation of Li_3N. On the other hand, there is an oxidation peak at ~0.5 V, which might be induced by the extraction of Li^+ from Li_3N under the oxidation current. Therefore, ε-Ti_2N is suitable for the application of LIBs, and it exhibited discharge capacity of ~450 mA h/g, which is close to the theoretical value. Besides, conversion-based materials also face the problems of low conductivity and large volume expansion similar to alloying-type materials [68]. The constructing nanocomposites (*e.g.* M_aX_b/graphene) is regarded as an effective method to improve electronic conductivity and alleviate huge volume changes during the discharge/charge cycles. For example, the Co_3O_4 has attracted much attention because of the high theoretical lithium-storage capacity (890 mA h/g), in which the eight Li^+ can be inserted into single lattice of Co_3O_4 during the lithiation process [69, 70]. Long *et al.* [71] recently fabricated Co_3O_4/graphene nanocomposites by a low pressure

capacitively-coupled-plasma (CCP) treatment (**Figure 4d**). In the CCP discharge device, the RF source is used to ionize Ar gas to generate high-energy electrons/ions flow, which strike onto the Co_3O_4 nanoparticles, and make them uniformly implanted into graphene nanosheets. The graphene plays a supporter role in the unique nanocomposites, while improving the electronic conductivity and shortening the path of Li^+ diffusion. Therefore, the plasma-treated Co_3O_4/graphene nanocomposites have high specific capacity (1368 mA h/g at 125 mA/g), excellent cyclability and rate capability.

Although conversion reactions could deliver remarkably high-capacity values, conversion-based materials also suffer from rapid capacity fading due to the structural deterioration upon charge/discharge process. The heteroatom doping engineering is regarded as an effective method to endow a highly stable linkage and improve the microstructural stability [72]. For example, Liu *et al*. [73] recently reported a facile and controllable approach via RF O_2 plasma to prepare O-doped and defect-rich MoS_2 nanosheeets. As shown in **Figure 4e**, since the atomic weight of S is smaller than that of Mo atoms, S atoms preferentially move out of the structure to form lattice vacancies when attacked by high-energy O excited species during the plasma exposure. Consequently, the original Mo-S bonds are broken, and the doped O atoms to form lattice disordered Mo-O-C bonds. In addition, a large number of residual S vacancies without O substitution are obtained. As expected, the vacancies/defects generated by oxygen plasma treatment offer extra transport paths for Li^+ and larger surfaces for electrochemical reaction. Meanwhile, the formed Mo-O-C bonds can enhance the structural/microstructural stability during cycling. Therefore, the as-fabricated MoS_2 nanosheeets demonstrated greatly enhanced reversible capacities and rate capabilities, and a superior long-term cycle life in contrast to the pristine MoS_2 nanosheeets.

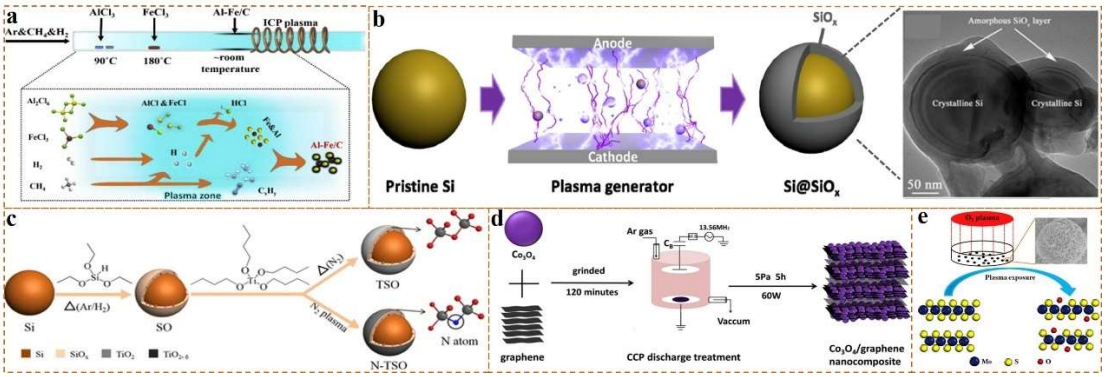

Figure 4. a) the schematic illustration of the reaction setup and the plasma reactions to from the Al-Fe/C nanocomposite. Reproduced with permission [57], Copyright 2020, Elsevier. b) Schematic illustration for the fabrication of Si@SiO_x through plasma oxidation, and the TEM image of Si@SiO_x. Reproduced with permission [63], Copyright 2021, Springer. c) the schematic illustration of N-TSO preparation. Reproduced with permission [62], Copyright 2019, American Chemical Society. d) the synthesis process of Co_3O_4/graphene nanocomposites by CCP discharge treatment. Reproduced with permission [71], Copyright 2017, Elsevier. e) the schematic diagram of the structural variation during the oxygen plasma treatment. Reproduced with permission [73], Copyright 2019, Elsevier.

4.1.1.2 Cathode materials

Layered $LiCoO_2$ is the first commercial cathode material for LIBs [74]. However, due to its low capacity, relatively high cost, toxic cobalt and unreliable safety, numerous

efforts have been made to develop alternative cathode materials. Until now, Li-containing cathode materials are divided into three categories according to Li^+ insertion/de-embedding channels: olivine structure $LiMPO_4$ (M=Fe, Mn, Co), layered structure $LiNi_xCo_yMn_zO_2$ (LNCM, x+y+z=1), and spinel structure $LiMn_2O_4$ (LMO) [75]. Meanwhile, the new cathode materials such as α-MoO_3, nickel sulfides (NS) have been also proposed. In this section, the plasma application for several cathodes as-mentioned above are described, and the influence of plasma on material structure/composition and properties are discussed.

(i) Olivine structure materials

Olivine structure $LiFePO_4$ (LFP) has been successfully commercialized due to high theoretical specific capacity (170 mA h/g), good thermal stability, environmental friendliness, and low cost. However, the poor conductivity and low Li^+ diffusivity are still the major problems [76, 77]. A practical method to improve the performance of LFP is to thoroughly coat it with a full conductive layer (*e.g.* carbon materials) and simultaneously reduce its particle size to nanoscale. For example, the porous active carbon-coated LFP nanoparticles (LFP/AC) in **Figure 5a** are successfully synthesized by *in-situ* N_2/H_2 plasma-assisted pyrolysis of the polyaniline (PANI) coating on precursor $FePO_4$ [78]. Compared with the normal calcination process, the *in-situ* plasma-assisted pyrolysis procedure can obtain a more desired graphitic structure as well as the porous structure. Interestingly, the homogeneous coating of PANI on precursor $FePO_4$ is helpful to control the size of produced LFP particles, which shortens the ion diffusion path, and converts to carbon network after pyrolysis to enhance the electronic conductivity, thereby enhancing the high capacity, rate capability and cyclic stability. In addition, Jiang *et al*. [79] synthesized $Fe•_{Li}$-antisite-free LFP nanoparticles with nitrogen-doped carbon coating (NC) and graphitic nanosheet support (GNS) using an Ar/H_2 plasma-assisted method. As shown in **Figure 5b**, the precursor (the PANI coated $FePO_4$), LiAc and sucrose are calcined to form LFP@NC, subsequent the mixture of LFP@NC, glucose and $FeSO_4$ is treated with H_2/Ar plasma, the plasma discharge not only promotes *in-situ* formation of GNS on LFP@NC via Fe^0-catalyzed glucose pyrolysis but also simultaneously removes $Fe•_{Li}$ antisites in LFP, and the $Fe•_{Li}$-antisite-free LFP@NC/GNS is thus obtained. The NC coating and GNS support can improve the Li storage kinetics and utilization of the active material, and the absence of the $Fe•_{Li}$ antisites can provide further expedited Li^+ diffusion paths in the LFP lattices, thereby allowing for ready migration of Li^+. The resultant LFP@NC/GNS showed enhanced reversible capacities, delivering a stable reversible charge/discharge capacity of 165.1 mA h/g at 0.2C, and a super-long cycling stability with no apparent capacity drop at 100 C for 1200 cycles.

(ii) Layered structure materials

$LiCoO_2$, is a high-cost and limited-capacity cathode material, and researchers have been promoting the substitution of Co with Mn and Ni to obtain layer structure LNCM [75]. However, the conventional co-precipitation and hydrothermal synthesis techniques require a reaction time scale of several hours, and they involve multiple steps and laborious processes, which is unfavorable for large-scale preparation of LNCM. In 2017, the LNCM was successfully synthesized by the atmospheric plasma-assisted method with ultra-fast processing time and ease of upscaling [80], and the process uses inexpensive precursors and does not need any post-synthesis treatment for obtaining crystalline LNCM. By altering the Ni/Mn/Co ratio in the precursor, the as-synthesized $LiNi_{0.2}Mn_{0.6}Co_{0.2}O_2$ cathode material delivered initial discharge specific capacity of

258 mA h/g, and 210 mA h/h after 50 cycles. However, the relatively low conductivity, and irreversible side reactions with electrolytes and cation (Li^+ and Ni^{2+}) are also still main challenges [81]. Surface coating is an effective way to address these problems [82]. For example, Jiang *et al.*[83] recently synthesized a uniform Al_2O_3-coated $LiNi_{1/3}Co_{1/3}Mn_{1/3}O_2$ with a hierarchical structure via O_2 plasma-enhanced low-temperature approach. As illustrated in **Figure 5c**, the $LiNi_{1/3}Co_{1/3}Mn_{1/3}O_2$ powder and aluminum isopropoxide ($C_9H_{21}AlO_3$, as the source of aluminum) are thoroughly mixed to form the precursor, and then the obtained precursor is treated by O_2 plasma to form $LiNi_{1/3}Co_{1/3}Mn_{1/3}O_2$ coated with Al_2O_3 (denoted as PLA-Al_2O_3@LNCM). The rate performance of PLA-Al_2O_3@LNCM is improved because of uniform Al_2O_3 coating on the surfaces of LNCM particles, which can delay the cathode/electrolyte interfacial reactions and facilitate Li^+ diffusion, especially at elevated temperature (93.6% capacity retention after 100 cycles at 55℃). Meanwhile, the Al_2O_3 layers can effectively suppress the growth of polarization resistance during cycling. Similar to above research, Chen *et al.* [84] developed a plasma-assisted milling method to prepare uniform SnO_2-coated $LiNi_{0.5}Co_{0.2}Mn_{0.3}O_2$ (NCM523) composites. The oxygen vacancy enriched SnO_2 nanoparticles are distributed on the surface of NCM523 particles under the interaction of plasma bombarding and mechanical milling. P-milling increases the discharge capacity of NCM523 and in the meanwhile the P-milled coating of SnO_2 greatly promotes the lithiation/delithiation kinetics, and stabilizes the NCM523 structure, as well as the active material/electrolyte interfaces. Thus, P-milled NCM523-SnO_2 composites exhibited a high initial Coulombic efficiency of 82.7% and a good capacity retention of 92.3% after 150 cycles.

(iii) Spinel structure materials

Spinel structure $LiMn_2O_4$ (LMO) has the characteristics of low cost, environmental friendliness, good thermal stability, high energy density, *etc*. [85]. The conventional high-temperature thermal annealing methods is well developed and utilized for the synthesis of LMO, but it requires prolonged heat treatment at relatively high temperatures (>750 ℃). In addition, this method has many disadvantages such as poor controllability of crystal growth, non-uniformity, irregular morphology, large particle size and wide distribution, *etc*. [86, 87]. For example, Jiang *et al*. [88] developed a O_2 plasma-enhanced low-temperature solid-state strategy to prepare spinel LMO (P-LMO). In comparison to the conventional high-temperature thermal annealing method, the synthesis temperature is reduced from >750 ℃ to 500 ℃. Meanwhile, as-prepared P-LMO showed fine particle size (400-450nm) and narrow distribution, with good electronic and ionic conductivity. Therefore, the P-LMO showed superior performance for LIBs in terms of initial discharge capacity and excellent cycling stability. However, the LMO also suffers from fast capacity fading during cycling due to the structural instability, Jahn-Teller distortion and Mn dissolution into the electrolyte [89]. As an example, the Ar plasma-assisted S-doping in LMO is performed by Jiang *et al.* [90] to obtain oxysulfide $LiMn_2O_{4-x}S_x$, in which the doped sulfur atoms occupy the oxygen sites in LMO to form the new bond Mn-S (**Figure 5d)**. The $LiMn_2O_{4-x}S_x$ has not only the similar cubic spinel structure to the pristine LMO, but also better crystallinity and uniform morphology than the pristine one. By comparison to pristine LMO, the as-prepared $LiMn_2O_{4-x}S_x$ showed higher specific capacity, and better rate capability. Specially, the cycling performance of $LiMn_2O_{4-x}S_x$ at the elevated temperature is dramatically enhanced, due to the suppression of Mn dissolution and the reduction of electrode resistance after the S doping.

(iv) Other cathode materials

The cathode materials that can store multiple electrons also attract great attention. For example, Yang *et al.* [91] proposed a solvent-free one-pot plasma reaction to synthesize morphology controllable nickel sulfides (NS) within minutes utilizing S-plasma and C-plasma. The S-plasma provided the sulfur source and high energy for the nickel foam substrates to generate NS with rapid kinetics, and the C-plasma containing plenty of C_2 radicals with high temperature can act on the reaction zone and adjust the morphology of nickel sulfides effectively. As shown in **Figure 5e**, by adjusting the composition of the plasma, the NS can be facilely shaped to columnar (pure S-plasma), stone-forest-like (introduce pure C-plasma after S-plasma) and sandpile-like (simultaneous introduce S-plasma and C-plasma). The as-synthesized NS exhibited good lithium storage performance as freestanding cathodes, especially the stone-forest-like NS delivers a high-rate capacity and superior cycling stability simultaneously. In addition, α-MoO_3 can reach high specific capacity great than 279 mA h/g (over 1.6 lithium per one transition metal) [92]. However, the capacity of α-MoO_3 decreases rapidly caused by its irreversible phase transition occurring at ~ 2.8 V [93]. In addition, the low electronic conductivity and slow reaction dynamics also limit its application [94].To this end, Zhang *et al.* [95] reported a controllable H_2 plasma etching approach for α-MoO_3 nanobelts to prepare α-MoO_{3-x}. XRD characterization certifies that the obtained α-MoO_{3-x} has reduced bandgap and expanded van der Waals gap, which further lead to reduced electron transfer resistance and improved efficient Li^+ diffusion. As a result, less polarization, increased structural stability, more reversible interlayer/intralayer Li sites and higher capacity are obtained. In additions, it was concluded that excessive etching (oxygen vacancy) by H_2 plasma has negative effects on microstructure, specific surface area and electron transfer resistance. Thus, moderate oxygen vacancies play a critical role in enhancing the electrochemical performance.

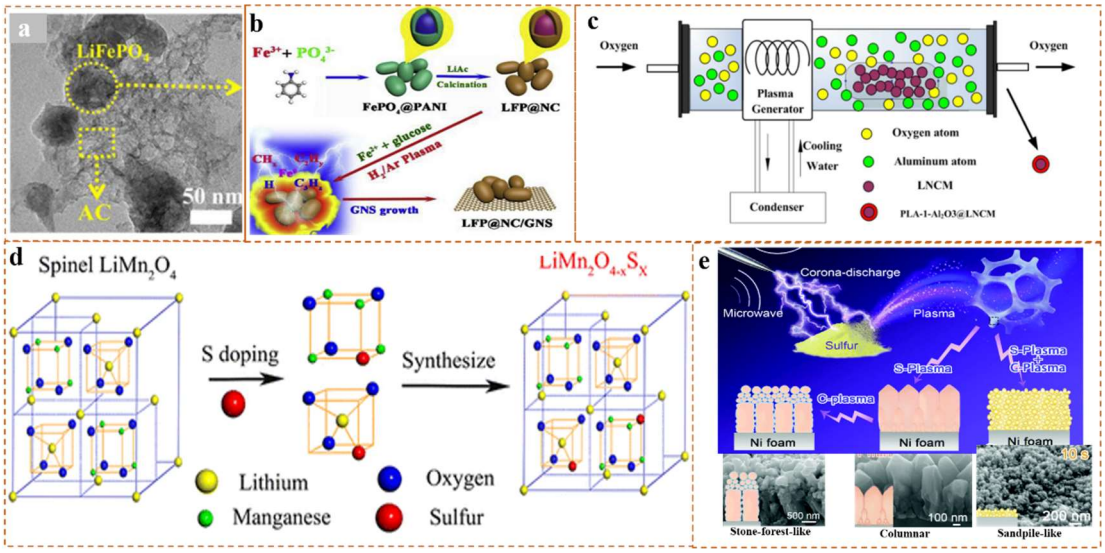

Figure 5. a) TEM image of LFP/AC. Reproduced with permission [78], Copyright 2020, Springer. b) the illustration of the synthesis process of LFP@NC/GNS. Reproduced with permission [79], Copyright 2019, Elsevier. c) the schematic diagrams for PLA-1-Al_2O_3@LNCM, d) TEM image of PLA-Al_2O_3@LNCM. Reproduced with permission [83], Copyright 2020, Frontiers. d) the structures of LMO and $LiMn_2O_{4-x}S_x$. Reproduced with permission [90], Copyright 2015, American Chemical Society. e) the schematic illustration of the solvent-free one-pot plasma reaction and the morphology-control of NS, and the SEM images and schematic illustration of the cross-section of stone-forest-like NS, columnar NS, and sandpile-

like NS. Reproduced with permission [91], Copyright 2020, Royal Society of Chemistry.

Table 3. Summary of synthesis/modification of electrode materials in LIBs by plasma technologies

Devices	Materials	Type of Plasma	Effects	Ref
LIBs (Anode)	TiO_2/C	RF plasma, Ar-N_2	Introduce OVs and Ti^{3+} ions	[46]
	TiO_2 nanowires	RF plasma, H_2	Introduce Ti^{3+} ions	[47]
	LTO	RF plasma, Ar-N_2	Introduce OVs and Ti^{3+} ions	[50]
	LTO	Glow Plasma, H_2-N_2	Introduce OVs	[51]
	g-C_3N_4	Glow plasma, H_2	Introduce NVs	[52]
	Al-Fe/C	RF plasma, Ar-H_2-CH_4	Synthesis	[57]
	Si@SiO_x	DBD Plasma, Atmospheric	Oxidation	[63]
	Si@SiO_x@$TiO_{2-\delta}$	RF plasma, N_2	N-doping	[62]
	ε-Ti_2N film	RF plasma, N_2	Synthesis	[67]
	Co_3O_4/graphene	RF plasma, Ar	Synthesis	[71]
	MoS_2 nanosheeets	RF plasma, O_2	O-doping /S vacancies	[73]
	AC-coated LFP	RF plasma, N_2-H_2	Plasma-assisted pyrolysis	[78]
	N-doped carbon-coated LFP	RF plasma, Ar-H_2	Plasma-assisted pyrolysis	[79]
LIBs (Cathode)	LNCM	Microwave plasma, Atmospheric	Synthesis	[80]
	Al_2O_3-coated LNCM	RF plasma, O_2	Oxidation	[83]
	SnO_2-coated LNCM	Glow plasma, N_2	Plasma-assisted milling	[84]
	LMO	RF plasma, O_2	Synthesis	[88]
	S-doped LMO	RF plasma, Ar	S-doping	[90]
	Morphologically-controlled nickel sulfides	Microwave/Corona plasma	Synthesis	[91]
	α-MoO_3	RF plasma, H_2	Etching /Introduce OVs	[95]

4.1.2 Sodium/Potassium-Ion Batteries (SIBs/PIBs)

LIBs, the front-runner for applications in portable electronic devices and electric vehicles, have begun to penetrate the grid-scale stationary electric energy storage market. However, the scarcity of Li pushes people to seek other alternatives [96].

Compared to Li, both sodium (Na) and potassium (K) are abundant in the earth's crust worldwide (0.0017, 2.3, and 1.5wt% for Li, Na and K, respectively [97]). Meanwhile, the price of metals, carbonates, or layered oxides of Na and K are all much cheaper than those of the corresponding Li compounds. Therefore, both sodium-ion batteries (SIBs) and potassium-ion batteries (PIBs) are considered suitable alternatives for LIBs [98, 99]. Moreover, the working principle of SIBs and PIBs is similar to that of the LIBs system, which is a "rocking chair model" based on Na-ions and K-ions insertion into the electrode materials [100], giving vast designing space and commercial prospects. Massive efforts have been put into developing diverse high-performance anode materials. This section will review some typical researches on the application of plasma. Examples of anode materials include carbon-based, alloying-based, titanium-based materials, and metallic oxides/selenides. Meanwhile, the summary of synthesis/modification of electrode materials in SIBs/PIBs by plasma technologies have also been presented in **Table 4**.

(i) Carbon-based materials

Carbon-based materials, which have been considered as the potential anode materials for SIBs/PIBs due to their high electron conductivity, low cost, and electrochemical stability. However, the small lattice space and inherent surface inertia of carbon-based materials are unsatisfactory to store and transport Na^+ and K^+ [101]. Meanwhile, the stability of the solid electrolyte interface (SEI) also should be considered during the charge/discharge process [102]. To enhance the Na/K storage, the introduction of surface functional groups is an effective method. For example, hard carbon (HC) is cheap due to its easy accessibility but suffers from the hydrophobicity to the electrolyte and poor cycling stability. Xie *et al.* [103] applied O_2-plasma treatment strategy to improve the wetting behavior through introducing oxygen functional groups (carbonyl and hydroxyl groups) on HC microspheres, which improves the ion diffusion coefficient. Meanwhile, the oxygen groups also provide more sites for Na^+ storage. Furthermore, as shown in **Figure 6a**, these interfacial oxygen groups exhibited less chemical activity toward electrolyte, inhibiting the decomposition of the electrolyte, while showed a stable performance due to the strong interaction between the ether or carbonyl groups and the SEI film. This benefits the ion/charge transport and achieving a more stable cycle performance and faster charge/discharge under higher current densities, thus leading to a higher capacity of 325mA h/g (the 225mA h/g for the pristine HC). Similar to above research, the N-doped carbon nanofiber with oxygen-rich functional groups have been successfully fabricated by O_2 plasma treatment for PIBs [104]. The surface oxygen-rich functional groups augmented surface storage of K^+ compared to N-doped carbon nanofiber. Meanwhile, the graphitic interlattice spacing increased from 0.37 to 0.46 nm owing to the N doping, and the architecture accommodated significant material expansion upon K^+ intercalation. Therefore, the electrode materials show superior cycling stability and coulombic efficiency due to the pseudocapacitive storage mechanism and the stable carbon architecture.

Heteroatom doping (*e.g.* S doping [101], N doping [105]) is another effective method to increase the electrochemical properties of carbon-based materials. As an example, Jiang *et al.* [106] developed a low-temperature Ar plasma enhanced chemical vapor deposition (PECVD) strategy to synthesize nitrogen/sulfur dual-doped graphitic hollow architectures (NSG) for PIBs. As shown in **Figure 6b**, the enlarged interlayer spacing and numerous defects owing to the N/S dual-doping are in favor of facilitating the adsorption, diffusion, and intercalation of K^+. Meanwhile, the hollow architectures of NSG endow it with structural stability, in turn accommodating the volume change of

graphitic layers during the charging and discharging. As a result, NSG manifests high-performance potassium storage, including favorable rate capability (≈100 mA h/g at 5 A/g) and outstanding cyclic stability (the capacity retention rate of 90.2% at 5 A/g after 5000 cycles).

(ii) Alloying-based materials

Alloy-based anodes, such as Sn-based materials [107] (*e.g.* Sn, SnS, and SnO) and P-based materials [108] (*e.g.* P, Sn_3P_4, SnP_3, and Se_4P_4) have been extensively reported to possess enhanced Na/K storage capacity. However, the rate performance and cycling stability are still a major bottleneck due to the severe volume expansion/contraction during the alloying/dealloying [109]. Some researchers [108, 110] introduced highly conductive elements (*e.g.* Sn, Se) to enhance the overall conductivity of P anode material, restrain the volume expansion, and avoid the formation of polyselenide during charge/discharge process. For instance, the plasma-assisted ball milling method not only offers a simple, cost-effective, and pollution-free method for preparing nanomaterials, but also accelerates mechano-chemical reactions to pave the way for the future large-scale production of composites. Lin *et al.* [111] applied the Ar plasma-assisted ball milling method to prepare the selenium-phosphorous-carbon (Se-P-C) amorphous composites for PIBs. As shown in **Figure 6c**, the mechanical energy, electron impact and heating impact are generated and exerted on the powder of Se, P, and graphite during the P-milling process. Meanwhile, the exfoliation and grind of graphite produces amorphous carbon. Consequently, carbon coated Se-P composite nanoparticles structure can be *in-situ* formed. When the molar ratio of Se to P is 1:2 and the ideal P-milling time is 30 h, the corresponding Se-2P/C amorphous composite anode showed the best electrochemical performance. This is attributed to the smallest particle size, which shorten the diffusion distance of K^+, and sufficient reaction between Se and P to form Se-P amorphous phase which not only enhances the conductivity of electrode material but also avoids the production of polyselenide in discharge/charge process. Specifically, the reaction mechanisms of the Se-2P/C have been revealed as the formation of new K-P (K_2P_3) and K-Se (KSe) phases during the potassiation process. More specifically, the corresponding potassiation/depotassiation mechanism for Se-2P/C material can be described by the following equation: $3(Se\text{-}2P) + 7K \leftrightarrow 3KSe + 2K_2P_3$.

In addition, the reasonable composite design of alloy-based materials and graphene (adapt to large volume changes, stable structure, and provide conductive channels) is an effective strategy. For instance, Chao *et al.*[107] proposed a rapid (5 min) carbon-plasma method to uniformly grow hierarchical graphene (hG) *in-situ* bundles on SnS nanobelt networks, to obtain unique flexible hG@SnS bundles membrane materials for SIBs. The schematic illustration and their structural evolutions of three electrode materials are shown in **Figure 6d**. Pure SnS nanobelts network undergoes severe pulverization and aggregation, and the exposed cracks offer fresh sites for the growth of thick and passivating SEI layer, accounting for conductivity decrease and large irreversible capacity fading. Although the rGO/SnS laminate composite film provides a protective cover for SnS with improved electric conductivity, poor cycling stability is still serious due to free volume expansion, particle detachment from rGO, and gradually deteriorated reaction kinetics. By contrast, chemical-bonded hG bundle serves as a conductive buffering framework, which effectively restricts the active materials reaggregation and thus stabilizes the structure, allowing an ultralong cycle life and high-rate performance, and the hG@SnS showed high volumetric and areal capacities with

excellent cyclic stability.

(iii) Metallic oxides/selenides

As mentioned above, the low conductivity of metal oxide/selenide needs to be overcome urgently. For example, the theoretical capacity of Fe_2O_3 is as high as ~1007 mA h/g, but the low electrical conductivity (10^{-14} S/cm) and low ionic diffusivity limits the rate performance of batteries [112, 113]. Because another iron-based oxide, Fe_3O_4, has a much higher electrical conductivity (10^2~10^3 S/cm) than Fe_2O_3 [114], Chang *et al.* [115] recently designed a Fe_2O_3/Fe_3O_4 nano-aggregates anchored on nitrogen-doped graphene (Fe_2O_3/Fe_3O_4/NG) by a microwave Ar/H_2 plasma process. As shown in **Figure 6e**, the Fe_2O_3/Fe_3O_4/NG composite exhibited rich phase boundaries and voids under the interaction of plasma bombarding. The highly conductive Fe_3O_4 in the composite can work as a highway of electron transport, and the voids and phase boundaries facilitate Na^+ diffusion into the nano-aggregates. Furthermore, the Fe-O-C bonds between the nano-aggregates and graphene not only stabilize the structural integrity, but also enhance the charge transfer. As a result, the Fe_2O_3/Fe_3O_4/NG composite showed high specific capacity, excellent cycling stability, and superior high-rate capability. In addition, bimetallic selenides (*e.g.* Co_2Mo_3Se [116]) have been investigated as a promising class of electrode materials because of their higher electrochemical activities and capacities than single-metal selenides (*e.g.* $CoSe_2$ [117], $NiSe_2$ [118]). For example, Zhang *et al.* [119] recently designed 3D $CoMoSe_4$ nanosheet arrays on network fibers of a carbon cloth ($CoMoSe_4$@C). As shown in **Figure 6f**, the 3D $CoMoO_4$ nanosheet arrays on network fibers of a carbon cloth ($CoMoO_4$@C) is first synthesized for SIBs. Subsequently, the $CoMoO_4$@C is treated with the N_2/H_2 plasma-assisted selenization at a low temperature, which O atoms can be replaced by Se atoms without the degradation on morphology. Meanwhile, the carbon cloth material with highly textured surface and good electrical conductivity is a good support, which can enable fast electron transport and buffer volume changes. Therefore, the $CoMoSe_4$@C showed a highly reversible capacity (475 mA h/g at 0.1 A/g) and excellent rate capabilities than that of the unselenized $CoMoO_4$@C.

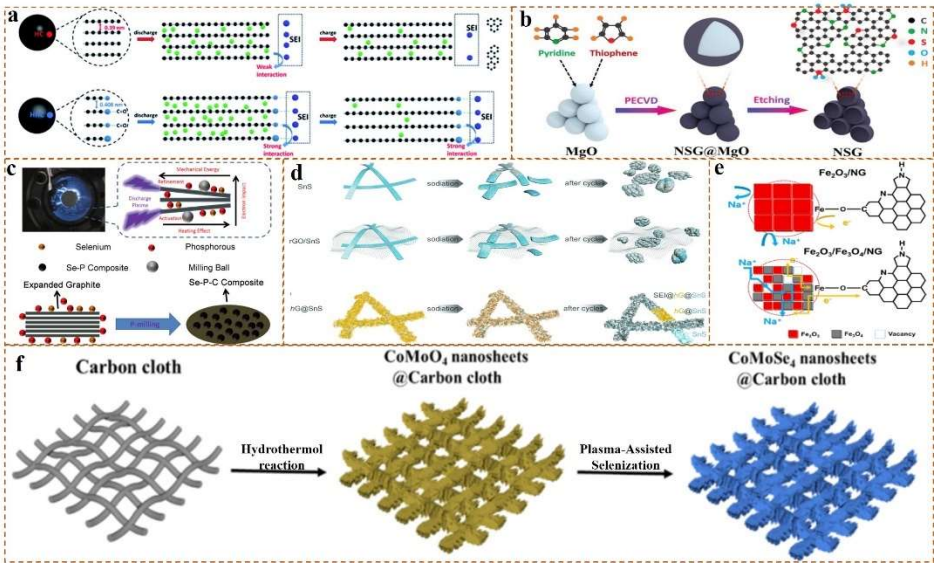

Figure 6. a) the schematic illustration mechanism of HC and HHC, the green circles represent sodium atom and the purple circles represent electrolyte molecules. Reproduced with permission [103], Copyright 2020, Royal Society of Chemistry. b) the schematic illustration of direct PECVD growth of NSG over MgO template.

Reproduced with permission [106], Copyright 2020, Wiley-VCH. c) the schematic illustration of the Se-P-C composite preparation. Reproduced with permission [111], Copyright 2019, Elsevier. d) the schematic illustration of three types of electrode configurations (SnS, rGO/SnS and hG@SnS) and their structural evolutions. Reproduced with permission [107], Copyright 2018, Wiley-VCH. e) the schematic of structures, electron transfer and transport, and ion diffusion in Fe_2O_3/NG (up) and Fe_2O_3/Fe_3O_4/NG (down) composites. Reproduced with permission [115], Copyright 2020, MDPI. f) the schematic diagram of the fabrication processes of 3D $CoMoSe_4$@C. Reproduced with permission [119], Copyright 2019, Springer.

(iv) Titanium-based materials

Apart from the aforementioned anode materials for LIBs, Ti-based materials (*e.g.* $NaTi_2(PO_4)_3$, zigzag layered $A_2Ti_nO_{2n+1}$(A =Na, K), and TiO_2) also are promising anode material for SIBs/PIBs. Nevertheless, the poor conductivity is still the major bottleneck. As mentioned above in the research [46], the incorporation of OVs is an effective way to accelerate the transport of electrons and ions. For example, Gan *et al.* [120] recently designed an urchin-like N-doped carbon coated anatase TiO_2 enriched with OVs (NC-DTO) through a facile hydrothermal method followed by Ar/H_2 plasma treatment, as shown in **Figure 7a**. The OVs in TiO_2 bulk can effectively enhance the intrinsic electronic conductivity of TiO_2, as well as accelerate Na^+ mobility in the TiO_2 host. Meanwhile, the as-synthesized ultrathin nanoflakes of the stable 3D urchin-like TiO_2 can provide shortened paths for Na^+ diffusion. Moreover, the N-doped porous carbon outside the TiO_2 with OVs can substantially improve the electronic conductivity as well as restrict volumetric expansion during the sodiation/desodiation process. Therefore, the NC-DTO exhibits a decent reversible capacity (272 mA h/g at 0.25 C), and the NC-DTO also reveals brilliant cycling stability. Furthermore, the zigzag layered $A_2Ti_nO_{2n+1}$(A =Na, K), which alkali-ions act as pillars between TiO_6 octahedron layers. As a member of them, the $A_2Ti_6O_{13}$(A =Na, K) with tunnel structures are favorable for Na^+ intercalation [121, 122]. As an example [123], the black $K_2Ti_6O_{13}$ nanowires are successfully fabricated by a hydrothermal method, followed by the as-prepared $K_2Ti_6O_{13}$ nanowires are reduced by H_2 plasma. The results of the first-principles calculations suggest that the electrical conductivity of B-KTO would be improved, and the sodiation energy barrier could be reduced after introducing OVs by H_2 plasma. The B-KTO electrode delivers a high capacity of 249 mA h/g at 0.1 C and 103 mA h/g at 20 C. Furthermore, it can sustain 20000 cycles in half cells at 20 C without obvious capacity decay.

Some researchers have proposed that heteroatom doping and introducing defects are a great way to improve the electrochemical performance of TiO_2 anodes [124, 125]. Meanwhile, the defect-rich phase can improve the solubility of dopant atoms, consequently not only achieve a higher doping level, but also enhance ion/electron diffusion. For example, Wang *et al.* [126] synthesized nitrogen doped and defect-rich TiO_2 materials by a highly efficient N_2 plasma assisted strategy. Much higher surface area than that of pristine TiO_2 greatly facilitated the Na^+ diffusion. Moreover, N-doping and abundant OVs are achieved simultaneously, leading to highly enhanced intrinsic electronic conductivity and facilitated Na^+ diffusion kinetics, and hence this electrode exhibited significantly improved reversible capacity and superior rate capability. Similar to the above research, a plasma-assisted method is reported to synthesize surface-defect-rich and deep-cation-site-rich S doped rutile TiO_2 (R-TiO_{2-x}-S) [127], as shown in **Figure 7b**, an ultrathin surface amorphous shell (≈3 nm) is induced by the Ar/H_2 plasma to bring the subsequent high S doping concentration (≈4.68 at%) and

deep doping depth, which highly improved intrinsic electronic conductivity and accelerated Na^+ diffusion kinetics. The advantages of the designed structure result in high reversible capacity, and outstanding long-term cycling stability and rate capability of R-TiO_{2-x}-S.

In addition, the conductive carbon coating on Ti-based materials is another feasible strategy to efficiently boost the conductivity. For instance, Cai *et al.* [128] recently reported a defective graphene-armored TiO_2 nanotubes (G-TiO_2 NTs) by direct plasma-enhanced chemical vapor deposition (PECVD) using CH_4 as the carbon precursor. As shown in **Figure 7c**, the defective graphene is *in situ* formed on the TiO_2 NTs surface at a relatively low growth temperature (~500°C), which endows TiO_2 NTs outstanding electrical conductivity. Meanwhile, the PECVD procedure allows the creation of topological defects within graphene overlayers, in turn helping easy permeation of electrolyte and fast intercalation of electrons/K-ions. Therefore, the armored graphene shells effectively buffer the volume change of TiO_2 upon potassiation/depotassiation, thereby delivering excellent pseudocapacitive K storage performance. In additions, conductive carbon coating has been also used to improve the electrical conductivity of $NaTi_2(PO_4)_3$ (NTP), which is considered as a Na super ionic conductor material, due to an open 3D framework, high ion conductivity, high theoretical capacity (133 mA h/g), low cost, and controllable easy synthesis [129-131]. For example, as shown in **Figure 7d**, an *in-situ* graphene growth on the surface of NTP nanoparticles by a PECVD strategy using CH_4 as the carbon precursor [132]. The monodisperse NTP nanoparticles with regular morphology and uniform size distribution are uniformly and completely covered by graphene. The as-obtained NTP@graphene (NTP@Gr) structure not only prevents the NTP particles from directly contacting the electrolyte, but also prevents Ti ions from dissolving into the electrolyte. Meanwhile, the agglomeration of NTP particles is avoided, and the diffusion path of Na ions and electrons is shortened, which will improve the ion conductivity. More importantly, the branched graphene protruding from the NTP@Gr further promotes electron transport between particles and electrodes. Therefore, NTP@Gr nanocomposite shows high-rate reversible capability, high initial coulombic efficiency (93%), and long-term capacity retention.

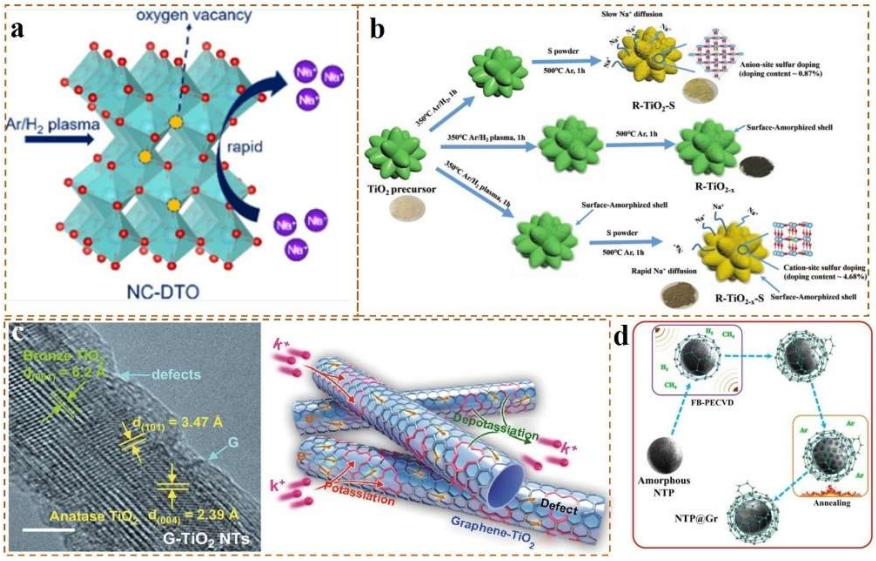

Figure 7. a) the schematic mechanism of NC-DTO. Reproduced with permission [120], Copyright 2018, American Chemical Society. b) the synthesis process for R-TiO_2-S, R-TiO_{2-x}, and R-TiO_{2-x}-S. Reproduced with permission [127], Copyright 2018, Wiley-VCH. c) HRTEM image of as-prepared G-TiO_2 NTs, and the schematic

showing electron/K-ion transport within G-TiO_2 NTs. Reproduced with permission [128], Copyright 2020, Springer. d) the schematic for the synthesis of NTP@Gr nanocomposite. Reproduced with permission [132], Copyright 2020, Royal Society of Chemistry.

Table 4. Summary of synthesis/modification of electrode materials in SIBs/PIBs by plasma technologies

Devices	Materials	Type of Plasma	Effects	Ref
SIBs	Hard carbon	RF plasma, O_2	Introduce oxygen functional groups	[103]
	Hierarchical graphene@SnS	RF plasma, CH_4	Carbon coating	[107]
	Fe_2O_3/Fe_3O_4/N-doped graphene	Microwave plasma, Ar-H_2	Synthesis	[115]
	$CoMoSe_4$@carbon cloth	Glow plasma, N_2-H_2	Plasma-assisted selenization	[119]
	N-doped carbon-coated TiO_2	Glow plasma, Ar-H_2	Introduce OVs	[120]
	N-doped TiO_2	Glow plasma, N_2	Introduce OVs /N doping	[126]
	S-doped TiO_2	Glow plasma, Ar	S-doping	[127]
	$K_2Ti_6O_{13}$ nanowires	RF plasma, Ar/H_2	Introduce OVs	[123]
	$NaTi_2(PO_4)_3$@ graphene	Microwave plasma, CH_4	Carbon coating	[132]
PIBs	N-doped carbon nanofiber	RF plasma, O_2	Introduce oxygen functional groups	[104]
	N/S dual-doped graphitic	Glow plasma, Ar	N/S dual-doping	[106]
	Se-P-C amorphous composites	Glow plasma, Ar	Synthesis	[111]
	Graphene-armored TiO_2 NTs	RF plasma, CH_4	Carbon coating	[128]

4.1.3 Metal-based Batteries

Metal-based batteries using metal (*e.g.* Li, Na, K, and Zn) as functional anodes are also among the most popular candidates for portable electronic devices and storage systems because they are able to store a large amount of energy per unit mass or volume. For instance, the theoretical capacity of Zn metal anodes can reach 5851 mAh/cm^3 or 820 mAh/g [133], and Li, Na and K metal anodes also have a high theoretical gravimetric

capacity of 3860, 1165 and 687 mAh/g, respectively [134-136]. Moreover, the metal anodes can pair with low-cost, high-energy, and non-side reaction cathodes (*e.g.* sulfur, manganese dioxide and oxygen), and can provide higher storage capacity compared with commercial LIBs [137]. However, dendrite growth inevitably appears on metal anodes since their formation is favorable in thermodynamics. This causes rapid capacity fade and short cycling capability, which limits large-scale and commercial application of metal-based batteries [138]. Plasma technologies have been applied for modification of metal anodes to address the above problems. This section will review some typical researches on the application of plasma for metal anodes. Meanwhile, the summary of modification of metal anode by plasma technologies have also been presented in **Table 5**.

4.1.3.1 Zinc Metal Anodes

Formation of Zn dendrites during Zn stripping/plating processes can cause sudden death of zinc metal batteries. Improving the surface zinc-affinity of Zn metal anode is an effective strategy to realize dendrite-free Zn plating performance. Jia *et al.* [139] reported a plasma-induced N-doping strategy to form N-doped interface on Zn metal anode (denoted as N-Zn). By virtue of N_2 plasma bombardment, uniform N doping on the surface of Zn metal anodes were achieved, which led to the improved electrical conductivity and even more active sites for Zn nucleation. As illustrated in **Figure 8a**, benefitting from the strong binding force between Zn^{2+} and N, the Zn^{2+} ions are preferred to evenly distribute on the N-Zn electrode, which thereby ensures the formation of fine and depressed Zn nuclei, resulting in an expected dendrite-free Zn plating process. In contrast, the bare Zn metal anodes surface formed severe Zn dendrites. Therefore, the symmetric cell of N-Zn electrode achieved an ultra-stable lifespan of 3000 h (1.0 mAh/cm^2 at 1.0 mA/cm^2). Moreover, the Zn//MnO_2 full battery also exhibited ultra-stable cycling behavior for 2000 cycles at 1.0 A/g.

Another effective way to achieve homogeneous Zn deposition is to cover it by a conductive coating with preferred-orientation of crystal planes on the Zn metal surface. For example, the rolled Zn flakes exposed more (002) crystal plane, and hence the better batteries performance [140]. Recently, a uniform $AgZn_3$ alloy layer coated Zn foil (denoted as $AgZn_3$@Zn) can be obtained by Ar plasma sputtering of the Ag target [141]. As shown in **Figure 8b**, the $AgZn_3$@Zn (002) particles are highly matched with the Zn (002) flakes, which can guide Zn form small and uniform flakes on the $AgZn_3$ surface. Then, Zn epitaxially grows horizontally and vertically to achieve uniform and dense Zn deposition. The $AgZn_3$@Zn symmetrical cell can exhibit high plating/stripping reversibility and long-term cycle life of 1360 h (1.0 mAh/cm^2 at 2.0 mA/cm^2), Moreover, the assembled $AgZn_3$@Zn||VO_2(B) full battery also exhibited ultra-stable cycling behavior for 2500 cycles (≈1500 h) at 0.5 A/g.

4.1.3.2 Alkali Metal Anodes

Dendrite growth is a ubiquitous problem for all alkali metal (*e.g.* Li, Na and K) anodes due to its high reactivity with electrolyte. Thus, suppression of dendrites is critical for high-performance alkali metal batteries. The design of artificial passivation layers is one of the promising and important strategies for improving interface management between alkali metal and electrolyte, thus enhancing the stability of alkali metal batteries. For instance, Zhao *et al.*[142] demonstrated improved Li metal batteries performance by surface engineering of the Li metal using different plasma treatments . As shown in **Figure 8c,** Ar or H_2 plasma treatments can efficiently remove the native oxidized layers (*e.g.* LiOH, Li_2O and Li_2CO_3) from the pristine Li metal surface thus

exposing the pure Li metal surface, where Ar plasma is more efficient than H_2 plasma. While O_2 plasma treatment produced Li_2O layer, N_2 or NH_3 plasma treatment formed Li_3N layer on the Li metal surface. These plasma-treated Li metals were used as the electrodes in Li-metal symmetric batteries. The Li_3N coated Li metal electrodes offered more stable performance and longer cycling life than those treated by other plasmas during the Li stripping/plating processes, indicating that Li_3N might serve as a protective coating layer to enhance the performance of Li metal batteries. In addition, Ardhi *et al.* [135] applied the amorphous polymeric carbon-based semiconducting passivation layers to Li-metal anodes using RF plasma thermal evaporation technology. The semiconducting characteristics and mechanical modulus of plasma-polymerized carbon layers (PCLs) were controllably adjusted from n-type to p-type semiconductor by increasing the RF plasma power from 0 to 300 W. A higher RF plasma power generates smaller carbon fragments and more carbon radicals, in turn leading to more oxygen-containing functional groups as defect-doping in the more amorphous PCLs and the controllably enhanced defect-doping change from n- to p-type. The n- and p-type semiconducting PCLs (n- and p-PCLs) form Ohmic and Schottky contacts with the Li-metal, respectively. Because p-PCLs enhanced the modulus and Li-ion conductivity, resulting in Li-ion deposition below the passivation layer, p-PCLs were more effective than n-PCLs at suppressing Li-dendrite formation (**Figure 8d**). Similar research work has been carried out in Na metal anodes. Luo *et al.* [134] applied a thin surface coating of Al_2O_3 on Na metal via a low-temperature O_2 plasma-enhanced atomic layer deposition (PEALD) process, which allowed atomically precise layer-by-layer growth of Al_2O_3 on Na metal. As shown in **Figure 8e**, the repeated plating/stripping cycles resulted in the formation of dendritic Na due to the unstable solid electrolyte interphase (SEI) formed on Na metal in carbonate electrolyte fails to effectively passivate the Na metal surface from the electrolyte. In contrast, the ultrathin coating of Al_2O_3 layers served as a stable artificial SEI on Na metal and resulted in a stable cyclic deposition/stripping process.

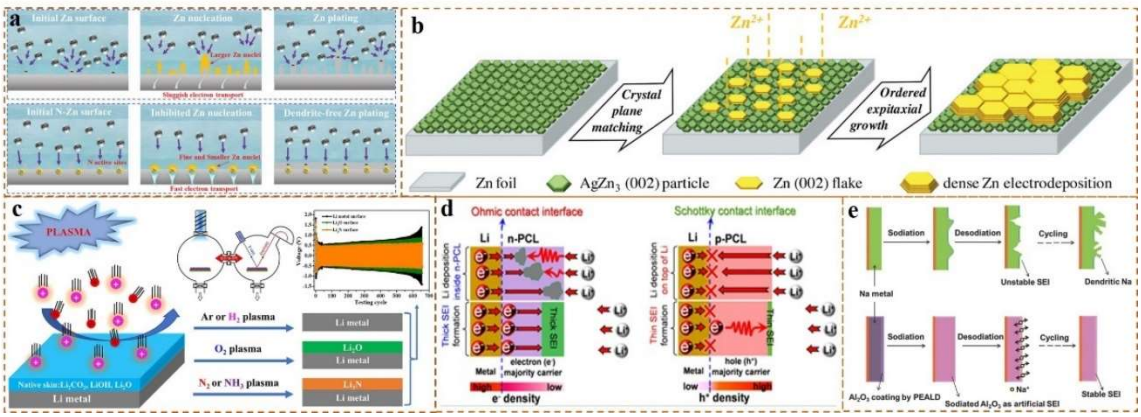

Figure 8. a) the schematic mechanism for different Zn nucleation and plating behaviors of Zn and N-Zn electrodes. Reproduced with permission [139], Copyright 2021, Wiley-VCH. b) the schematic of dendrite-free Zn deposition based on vertical crystal plane matching. Reproduced with permission [141], Copyright 2022, Wiley-VCH. c) the process scheme of pristine Li to obtain Li metal surface by Ar or H_2 plasma, Li_2O surface by O_2 plasma and Li_3N surface by N_2 or NH_3 plasma. Reproduced with permission [142], Copyright 2022, Elsevier. d) the schematic deposition behavior of Li-ions in n- and p-PCLs: deposited Li-metal inside the n-PCL and below the p-PCL, and thick and thin SEI layers on n- and p-PCLs, respectively. Reproduced with permission [135], Copyright 2021, American Chemical Society. e)

the schematic illustration of the stabilization of the Na metal anode by PEALD Al_2O_3 coating. Reproduced with permission [134], Copyright 2017, Wiley-VCH.

Table 5. Summary of modification of metal anode materials by plasma technologies

Devices	Materials	Type of Plasma	Effects	Ref
Metal-based batteries	Zn metal anode	Glow plasma, N_2	N-doping	[139]
		Glow plasma, Ar	Sputtering	[141]
	Li metal anode	Glow plasma, Ar/H_2/O_2/N_2/NH_3	Reduction/ Oxidation/ Nitridation	[142]
		RF plasma, Ar	Polymerization	[135]
	Na metal anode	Glow plasma, O_2	Oxidation	[134]

4.1.4 Supercapacitors (SCs)

Much attention has been attracted to develop advanced SCs with high energy and power density, good reversibility, and long cycle life. According to the charging/discharging mechanism of the electrodes, SCs are generally divided into (i) electrichemical double-layer capacitors (EDLCs) that depend on the adsorption/desorption of the electrolyte ions at the interface of the electrode/electrolyte double layer and (ii) pseudocapacitors that rely on the oxidation-reduction reaction to carry out the charge storage by the electron transfer process [143, 144]. However, the state-of-art electrode materials still have significant constraints and shortcomings, such as the low specific capacity of the EDLCs materials (mainly carbon materials) and the poor cycle stability of pseudocapacitance materials (transition metallic compounds [145-147], conductive polymers [148, 149] *etc.*). So far plasma has been successfully utilized to modify and fabricate the electrode materials for SCs. In this section, some typical application of plasma technology for various electrodes including carbon materials, pseudocapacitance materials, and carbon-based composites will be discussed. Meanwhile, the summary of synthesis/modification of electrode materials in SCs by plasma technologies have also been presented in **Table 6**.

4.1.4.1 Carbon Materials

Carbon materials are currently the most used electrode materials in EDLCs due to excellent electrical conductivity, good physical and chemical stability. Several reports [150-154] have successfully demonstrated enormous potential of plasma technologies. As a member of them, biochar also known as black carbon, is a byproduct of biomass pyrolysis. As a low-cost, environmental-friendly material, biochar has the potential to replace more expensive synthesized carbon nanomaterials (e.g., carbon nanotubes, graphene) for use in future supercapacitors. To achieve high capacitance, biochar requires proper activation. A conventional approach to produce hierarchical pores is to mix carbon materials with strong alkalis (e.g. KOH) and then bake them under harsh condition ($\geqslant$ 800 °C for several hours) [155]. However, this approach has many problems such as poor controllability, high pollution, low output, and long cycle *etc*. In

contrast, the environment-friendly plasma activation strategies (*e.g.* etching and sputtering effects) are efficient to significantly tune the microstructure (*e.g.* pore size distribution). For example, Gupta *et al*. [156] pyrolyzed the yellow pine biochar via a low-temperature (<150 °C) O_2 plasma to create micro-meso-macro-pores coexisting structure. The as-obtained biochar exhibited a much higher specific capacitance (171.4 F/g) than chemically activated biochar (99.5 F/g) and untreated biochar (60.4 F/g). Furthermore, Soundarya *et al.* [157] used the prosopis juliflora bark as precursor to prepare the 'plasma carbon' by plasma-synthesis method without any chemical activation. As shown in **Figure 9a**, the plasma carbon presents micro-mesoporous structure with the average pore diameter of 3.928 nm, larger than the size of solvated ions (K^+=2.8 Å and OH^-=1.33 Å) in KOH solution, thus facilitating the ion diffusion. Therefore, the plasma carbon electrode presented a high specific capacitance (193 F/g at 1.0 A/g), and the fabricated symmetric SC achieved an energy density of 22.0 Wh/kg at a power density of 600 W/kg. Similarly, Kumar *et al.* [158] have successfully prepared the hierarchical cauliflower-like VGNs (F-VGNs) by plasma-assisted process using coconut oil as precursor. The effective channels connecting the top surface to the interior provide effective paths for electrolyte ions to enter and exit the electrode materials. Thus, the F-VGNs electrode presents a high specific capacitance (312 F/g at 10 mV/s) with 100% retention after 1000 cycles, as well as extraordinary high-specific capacitance of 148 F/g at a high scan rate of 500 mV/s.

A major challenge is the poor wettability in electrolyte of carbon materials result in the low specific capacitance, which restricts their widely application. Generally, there are two predominant approaches to optimize carbon materials: (i) surface modification with oxygen-containing functional groups (*e.g.* hydroxyl -OH, carboxyl group -COOH, carbonyl group -C=O) [159] can result in enhancement of electrode surface wettability; (ii) surface modification with heteroatoms (*e.g.* N, O and P) [160] can provide more active sites [161]. The introduction of oxygen-containing functional groups through plasma has been proved as an efficient strategy to improve the wettability of carbon materials. For example, Adusei *et al.* [162] presented that the atmospheric pressure O_2 plasma treatment can increase the number of oxygen-containing functional groups on the CNTs surface. The specific capacitance of functionalized CNTs increased by 132.8% compared to non-functionalized CNTs. Furthermore, the capacitive characteristics of the multiwalled carbon nanotubes (MWNTs) are compared using the microwave treatment (m-MWNTs) and the O_2 plasma treatment (p-MWNTs) by Dulyaseree *et al* [163]. As shown in **Figure 9b**, the p-MWNTs exhibit the reduced contact angle due to oxygen-containing functional groups. The electrochemical results further revealed that p-MWNTs possessed improved specific capacitance and reduced intrinsic ohmic resistance (R_s). Similar treatments also convert the intrinsic hydrophobic vertical graphene nanosheets (VGNs) into super-hydrophilic ones [164], while preserve the unique 3D interconnected porous network, as shown in **Figure 9c**. The X-ray photoelectron spectroscopy (XPS) data proved that the surface oxygen content of VGN increased significantly after plasma treatment (both *ex-situ* and *in-situ*). *In-situ* means that the VGNs are unexposed to ambient before the plasma treatment. In contrast, the sample is exposed to ambient before the plasma treatment is called *ex-situ*. Moreover, the change of plasma power can effectively modulate the concentration of oxygen-containing functional groups. More importantly, under the same plasma power, *in-situ* plasma treatment VGNs found to consists higher -OH and -C=O functional groups (high thermal stability*)* compared to ex-situ plasma treatment. Therefore, *in-situ* plasma-treated VGNs electrode exhibited higher capacitance than *ex-situ* treated ones. And the areal capacitance of the VGNs electrode (1.7 mF/cm^2) *in-situ* plasma treated

at 600W reached 10 times over the inherent hydrophobic ones. In addition, carbon-based fibers (*e.g.* graphene fibers [165] and carbon nanofibers [166-168]) can also be decorated with more oxygen-containing functional groups by O_2-containing plasma, and achieve improved specific capacitance. Although the introduction of oxygen-containing functional groups into the carbon network can improve the wettability, excessive and unstable functional groups can result in low conductivity and rate performance. Chen *et al.* [38] reported that the graphene oxide (GO) nanosheets on the non-conductive polyethylene terephthalate substrate can be successfully reduced at a moderate temperature (100-200°C) by H_2/N_2 plasma, and the plasma treated sample shows higher conductivity. Subsequently, Song *et al.* [169] used the DBD Ar-plasma to reduce the surface oxygen content of graphene oxide nanoribbons to obtain the graphene nanoribbons (GNRs). The oxygen content decreased with increasing the treatment time due to the energy transfer with high-energy electrons/ions to produce oxygen-containing gases (*e.g.* CO, CO_2 and H_2O), in which unstable C-O-C functional groups are removed, or converted into more stable C-OH/C=O functional groups. Meanwhile, the plasma treatment can inhibit the aggregation of graphene oxide nanoribbons and expose more edge active sites. As a result, the as-obtained GNRs with suitable oxygen functional groups and inherent edge-enriched structure have exhibited high specific capacitance of 229 F/g at 0.5 A/g.

Heteroatom doping through plasma is another effective strategy to adjust the physical and chemical properties of materials. Especially the active sites and wettability of carbon materials can be increased by controlling the content and type of heteroatoms. For example, the dc-pulse N_2 atmospheric-pressure plasma jet (APPJ) possesses rapid processing capabilities for carbon materials due to the high reactivity, and has been used to modulate carbon materials. As shown in **Figure 9d**, Kuok *et al.* [170] used the 30s N_2 APPJ treatment to dope N in the CNTs on carbon cloth to improve the wettability. Meanwhile, the oxidation and evaporation of the organic binder take place to form a porous structure with a large surface area, which promotes electrolyte penetration and enhance capacitive behavior. Hsu *et al.* [171] also doped reduced graphene oxide (rGO) with minimized structural damage through N_2 APPJ treatment. As a result, the best achieved areal capacitance is 15.93 mF/cm^2, which is 3.6 times higher than that without APPJ treatment. Similar effects by N_2-containing plasma have been also verified for GO film [172], graphite oxide [173] and carbon cloth [174], in which the electrochemical active sites as well as the wettability can be significantly increased. Another way to achieve heteroatom doping is to treat heteroatom-rich precursors in plasma. For instance, the N-doped graphene was prepared by plasma exfoliation of polypyrrole-modified graphite oxide [175] (**Figure 9e)**. The doped N concentration depended strongly on the plasma feedstock. Compared with O_2 plasma and N_2 plasma, the CH_4 plasma promotes the incorporation of N in graphite oxide and/or produces more pyridinic-N, which can provide pseudocapacitance and improve conductivity. Therefore, CH_4 plasma exfoliated N-doped graphene exhibits better capacitance performance. Furthermore, the N-doped carbon nanofiber (N-P-CNF) is prepared by the ambient plasma treatment, followed by the thermal treatment with melamine as N precursor with melamine [176]. In comparison with CNF, the N-P-CNF exhibited the higher doping content of N (11 wt.%) and the electrochemical active surface area of N-P-CNF has increased by almost 4 times. Co-doping can further tune the overall properties compared with single heteroatom doping because of the synergistic effect between doped species [177-179]. As shown in **Figure 9f**, boron and nitrogen co-doped rGO (BN-rGO) [180] was prepared by the H_2-DBD plasma treatment. Compared to the single-doped B-rGO and N-rGO, the BN-rGO exhibited the highest doping content of

N (2.69 at.%) and B (1.47 at.%) due to the mutual promotion of N and B doping. Due to the similar atomic radius with C atom, the doping of B and N atoms has no damage to the overall structure of the carbon skeleton. More importantly, the two dopants have a synergetic effect due to the electron accepting nature of B and electron-donating nature of N. Therefore, the specific capacitance of BN-rGO is as high as 350 F/g, which is 2.36, 1.46 and 1.21 times higher than that of rGO, B-rGO and N-rGO, respectively. Furthermore, Miao *et al.* [181] prepared N/S co-doped rGO using the Ar/H_2 plasma treatment, in which the reduction and N/S co-doping are achieved simultaneously. N and S atoms can be uniformly doped into the graphene nanosheets. The doped N provides more chemically active sites for a higher capacity, and the doped S can broaden the band gap to benefit the fast access of ions at the electrode/electrolyte interface. Therefore, the plasma treated electrode exhibits high specific capacitance (307.4 F/g at 1 A/g), good cycling performance, and excellent conductivity.

Another major challenge is the undesirable morphologic structure of carbon materials result in the low specific capacitance, which restricts their widely application. Generally, the hierarchical porous structure of carbon materials is beneficial to provide large surface areas and accessible paths for electrolyte ions [144, 182]. For example, Xu *et al.* [183] successfully prepared a hierarchically porous carbon-coated SnO_2@graphene foams as anodes for LIBs, showing enhanced lithium storage properties. In addition, the dc-pulse N_2 APPJ is utilized to sinter rGO by Yang *et al.* [184]. Owing to the synergetic effect of the reactive species and heat flow, the APPJ-sintered rGO shows nano-porous structure to ensure large surface area for facilitating the penetration of the electrolyte into the nanopores

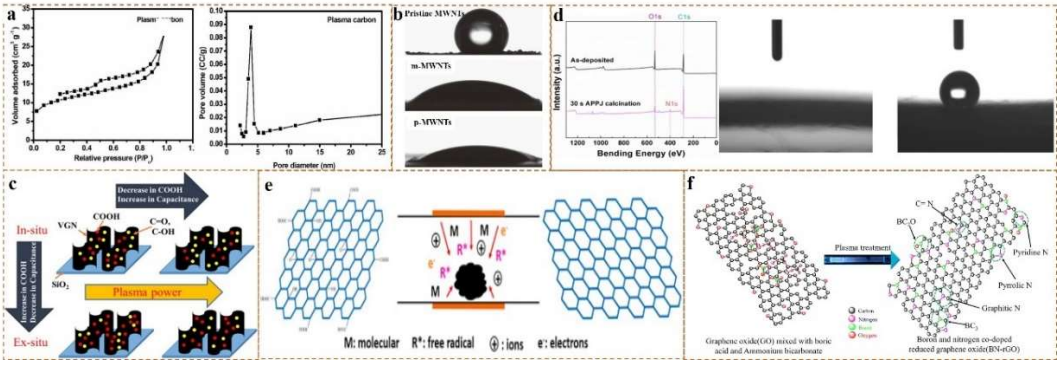

Figure 9. a) the SEM micrograph, N_2 adsorption isotherm and pore size distributions of the plasma carbon. Reproduced with permission [157], Copyright 2022, IOP. b) the water contact angles of pristine MWNTs, m-MWNTs, and p-MWNTs. Reproduced with permission [163], Copyright 2016, IOP. c) the schematic representation oxygenated functional groups attached to the plasma treated VGN surfaces. Reproduced with permission [164], Copyright 2018, Elsevier. d) XPS wide scan spectra of APPJ-calcined CNTs on carbon cloth, and the water contact angles of the APPJ-calcined (left) and as-deposited pastes (right). Reproduced with permission [170], Copyright 2017, Elsevier. e) the schematic illustration of plasma exfoliation. Reproduced with permission [175], Copyright 2017, Elsevier. f) the schematic of the synthetic procedure of BN-rGO. Reproduced with permission [180], Copyright 2019, Springer.

4.1.4.2 Pseudocapacitance Materials

Pseudocapacitance materials are attractive for SCs due to their much higher (typically 10-100 times) specific capacitance and energy density compared to those of carbon

materials. Especially, transition metallic compounds are mostly investigated because of their multiple valence states that enable fast surface faradaic redox reactions [185, 186]. Nonetheless, the transition metallic compounds that are currently available have many drawbacks (*e.g.* difficult to synthesize by conventional methods [187], low specific surface area [188] , and poor conductivity [189]), which limit their wider applications. The plasma technologies have been successfully applied to address these drawbacks.

Transition metallic phosphides exhibit promising electrochemical properties due to their high conductivity and stability [36, 190]. The high reactivity of P-plasma can rapidly convert the precursors to corresponding metal phosphides at low temperature, and it is difficult to synthesize the same phosphide by conventional methods. For example, the metal phosphides nanoplates are converted from the corresponding hydroxide using PH_3/He plasma-assisted method [187], as shown in **Figure 10a**. Using Ni_2P, CoP and NiCoP as a demonstration, it showed that the Co substitution into Ni_2P not only effectively altered the electronic structure and improved the intrinsic reactivity and electrical conductivity, but also stabilized Ni species when used as SCs electrode materials. The resultant NiCoP nanoplates have both the high capacity of Ni_2P and the good rate capability of CoP. Consequently, the as-assembled NiCoP nanoplates//graphene asymmetric SCs delivered a high energy density of 32.9 Wh/kg at a power density of 1301 W/kg, along with outstanding cycling performance, which is higher than most of NiCo-based asymmetric SCs.

Plasma etching can change the surface morphology of material films to increase their surface roughness and specific surface area. For example, high conductivity hafnium nitride (HfN) films are produced by directional etching in the Ar/Kr plasma [188]. Since the Kr atoms/ions possess higher mass and energy than the Ar atoms/ions, the weakly-bonded atoms at the sub-boundaries can be more easily resputtered or etched away by the heavier Kr ions, and thus the addition of Kr gas in the plasma could further increase the etching rate. As depicted in **Figure 10b**, the SEM images revealed that the plasma etching significantly enhanced the surface roughness of the HfN films without changing the phase structure. More importantly, the increase of adsorption sites after etching reduced the charge transfer resistance of the films. Therefore, the plasma etched HfN films achieved a relatively high capacitance of 5.6 mF/cm^2 at 1.0 mA/cm^2 with excellent cycling life, which is enlarged 8 times than that of the pristine films without plasma etching.

The incorporation of anion vacancies (*e.g.* OVs, selenium vacancies) through plasma is an effective method to improve the conductivity of transition metallic compounds. For example, as shown in **Figure 10c**, the micro-porous Co_3O_4 powders with high OVs concentrations are produced by active H_2 microwave plasma etching [191]. The SEM images in **Figure 10c(left)** showed that the pure Co_3O_4 powders are spherical in shape with a diameter about 7-8μm, which are consisted of particles roughly 100-300 nm in diameter with a lot of small holes between them. In contrast, the plasma treated Co_3O_4 (P-Co_3O_4) as shown in **Figure 10c(right)** revealed that the edges of the particles are much more pronounced, and the apertures have expanded further to form a hollow state. The results showed that the electrochemical performance of P-Co_3O_4 is 3.5 times better than that of the origin Co_3O_4 powders due to the increased OVs and the optimally adjusted ratio of Co^{2+}/Co^{3+}. In addition, Liang *et al.* [192] reported a PH_3 plasma activation strategy to activate the Fe_2O_3 but without changing the bulk phase. The plasma activation can effectively improve the OVs concentrations, which would improve the intrinsic conductivity and promote the reactivity of Fe_2O_3. Moreover, the *in-situ* generated surface phosphates and phosphides can also increase the active surface

area and participates in the surface faradaic redox reactions, and thus leading to a five-fold enhancement in areal capacitance for the plasma activated Fe_2O_3 (340 mF/cm^2 at 1.0 mF/cm^2) as compared with the pristine Fe_2O_3. Similarly, Cui *et al.* [193] recently reported the birnessite-MnO_2 with robust lattice OVs (LOV-MnO_2) by the H_2 plasma and O_2 plasma treatment, in which the H_2 plasma generates OVs in the entire MnO_2, and the subsequent O_2 plasma treatment leads to the healing of surface oxygen defects and residual lattice OVs. The as-obtained LOV-MnO_2 showed enhanced conductivity and electrochemically active sites. Therefore, the LOV-MnO_2 contributed to a specific capacitance (445 F/g) with remarkable capacitance retention (96.6%). The configured symmetrical SC also delivered remarkable performance with an energy density of 92.3 Wh/kg at a power density of 1100.3 W/kg, along with an outstanding cycling stability of 92.2%. Furthermore, the plasma-induced selenium vacancies have also been verified for improving conductivity. Specifically, as shown in **Figure 10d**, the lamellar $NiSe_2$-butylamine hybrid precursors are treated via Ar plasma-assisted exfoliation to form free-standing ultrathin porous $NiSe_2$ nanosheets with selenium vacancies ($NiSe_2$ PNS_{vac}) [194]. The generated selenium vacancies significantly increased the conductivity of $NiSe_2$ PNS_{vac} and promoted the transport of electrons. Meanwhile, the ultrathin porous structure effectively increased the specific surface area and shortened the diffusion path of electrolyte ions. As a result, the specific capacitance of the $NiSe_2$ PNS_{vac} can reach 466 F/g, which is much higher than that of $NiSe_2$ nanosheeets (328 F/g) and $NiSe_2$ particles (251 F/g).

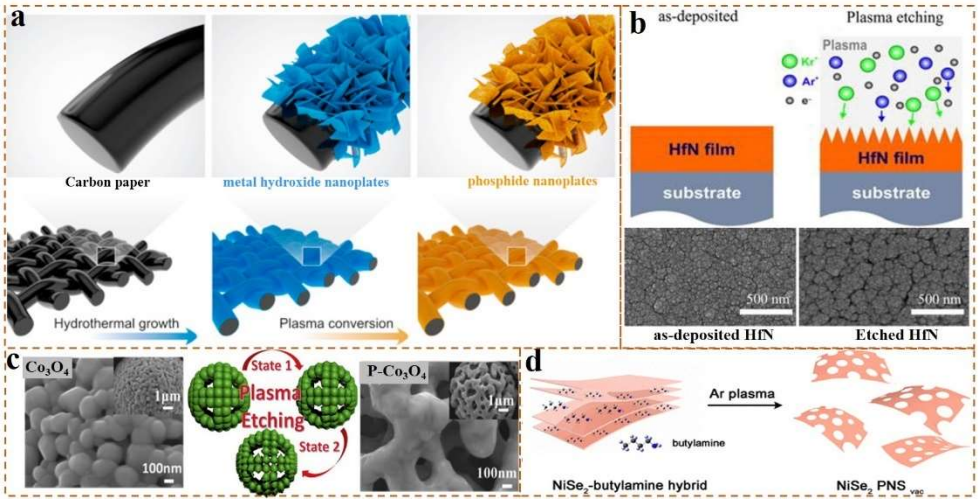

Figure 10. a) the schematic illustration of the synthetic process of metal phosphide nanoplates. Reproduced with permission [187], Copyright 2017, Elsevier. b) the schematic diagrams of the as-deposited and plasma-etched HfN films, and the surface SEM images of the as-deposited and plasma-etched HfN films. Reproduced with permission [188], Copyright 2019, Elsevier. c) the experimental schematic of plasma treatment, SEM images of pure Co_3O_4 (left) and P-Co_3O_4 (right). Reproduced with permission [191], Copyright 2019, Elsevier. d) the schematic procedure for the preparation of $NiSe_2$ PNS_{vac}. Reproduced with permission [194], Copyright 2018, American Chemical Society.

4.1.4.3 Carbon-based Composites

A hybrid nanostructured composite electrode integrating two electrode materials has been recommended as an effective way of alleviating various issues raised for individual candidates. For instance, the composite electrode including carbon materials

(*e.g.* CNTs, CNFs, carbon cloth, and rGO) as a host and pseudocapacitance materials (*e.g.* transition metallic compounds, conductive polymers) as a guest can not only have higher specific capacitance (*v.s.* carbon materials), but also have higher cyclic stability (*v.s.* pseudocapacitance materials), and many carbon-based composites electrodes have been reported for the fabrication of high performance SCs [195-199].

Many reports have demonstrated successful application of plasma technologies in the introduction of transition metal oxides into carbon materials. For example, as can be seen in **Figure 11a**, the Co_3O_4-incorporated multichannel carbon nanofibers (P-Co-MCNFs) composite electrode is prepared using O_2 plasma exposure by Kim *et al.* [200]. The Co_3O_4 particles are uniformly embedded in the multichannel CNFs structure without collapse. Benefit from the synergistic effect of the inner pore and the Co_3O_4 component, the as-obtained P-Co-MCNFs exhibited high specific capacitance (821 F/g at 1.0 A/g) with a remarkable cycling stability (92.1% over 5000 cycles). Moreover, the assembled P-Co-MCNFs-based symmetric SC also delivers a very high energy density (39.1 Wh/kg) with 89.9% capacitance retention after 5000 cycles. Recently, Chodankar *et al.* [201] developed an interface engineering strategy to prepare metallic oxides/carbon composites. As schematically shown in **Figure 11b**. the N_2 plasma-treated carbon cloth (NCC) exhibited superhydrophilic nature with a hierarchical nanostructure, which can provide a large surface area for electrochemical reactions as well as for hosting the electroactive material. Then, inorganic $NiCo_2O_4$ (NCO) nanowire arrays are deposited on the NCC. Finally, an ultrathin layer of NiO is deposited on the NCO nanowire arrays via atomic layer deposition (ALD). The ultrathin NiO layer can not only act as a buffer layer to prevent the damage of NCO nanowires during the long-term charge-discharge process, but also facilitate fast charge transfer and diffusion of the electrolyte ions to the NCO electrodes. The optimized NCC/NCO/NiO core-shell electrode exhibited a high specific capacitance (2439 F/g) with a remarkable cycling stability (94.2% over 20000 cycles). Moreover, the foldable solid-state SCs are fabricated with the excellent NCC/NCO/NiO core-shell nanowire array electrodes, and the device showed a high energy density of 72.32 Wh/kg at a specific capacitance of 578 F/g with excellent cycle stability. In addition, the SnO_2/CNTs [202] and Fe_2O_3/CNT [203] composites electrodes are also successfully prepared through dc-pulse N_2 APPJ treatment, and achieved improved electrochemical performance.

Apart from the transitional metal oxides, the introduction of conductive polymers into carbon materials through plasma technologies have also been verified. For example, as shown in **Figure 11c**, the polyaniline (PANI) is grafted onto the surface of highly conductive carbon nanofibers (PANI-P-1.0) via plasma polymerization [204]. The emeraldine base form of nanorod-polyaniline is well-distributed on the surface of the CNFs. The PANI-P-1.0 has a high specific capacitance of 606 F/g because the high capacitance is contributed by the electric double layer capacitance of CNF and the pseudocapacitance of the grafted PANI. In addition, the capacitance of the PANI-P-1.0 showed no decay after the 1000 cycles at 1.0 A/g because the free space around PANI allowed volumetric change and the strong interaction between PANI and CNF by covalent bonds. Similarly, CNTs are coated with ultra-thin PANI films (PANI/CNTs) through RF plasma polymerization [205], as-obtained PANI/CNTs electrodes delivered a specific capacitance of 1225 F/g. Moreover, the cycling stability testing demonstrated that the PANI/CNTs composite retained 65% of the initial specific capacitance (410 F/g) after 5800 cycles at 15.0 A/g current density. Besides PANI, polypyrrole (PPy) is also a widely used conductive polymer material. For instance, as depicted in **Figure 11d**,

Han *et al.* [206] recently used He plasma to etch carbon nanotube films (HCNTF) to produce amorphous carbon to improve the wettability of carbon nanotube films (CNTF). The improved wettability enhanced the adhesion between the PPy and the HCNTF, and promoted the electrodeposition of PPy onto HCNTF. The all-solid-state flexible SCs prepared based on the PPy/HCNTF electrodes exhibited a higher specific capacitance and better cycle stability than the PPy/CNTF electrodes. Similar, the surface of CNTs can be decorated with oxygen-containing functional groups through atmospheric plasma to enhance the dispersibility of CNTs [207]. More importantly, the pyrrolic nitrogen groups of PPy provided active sites for forming the conjugated structure, which enhanced the interaction between CNTs and PPy, and thus the PPy can be uniformly coated on the surface of CNTs to obtain PPy-bonded CNTs composites (PPy/P-CNTs). The PPy/P-CNTs exhibited a larger specific capacitance and better charge/discharge ability in comparison to the CNT/PPy and pure PPy electrodes.

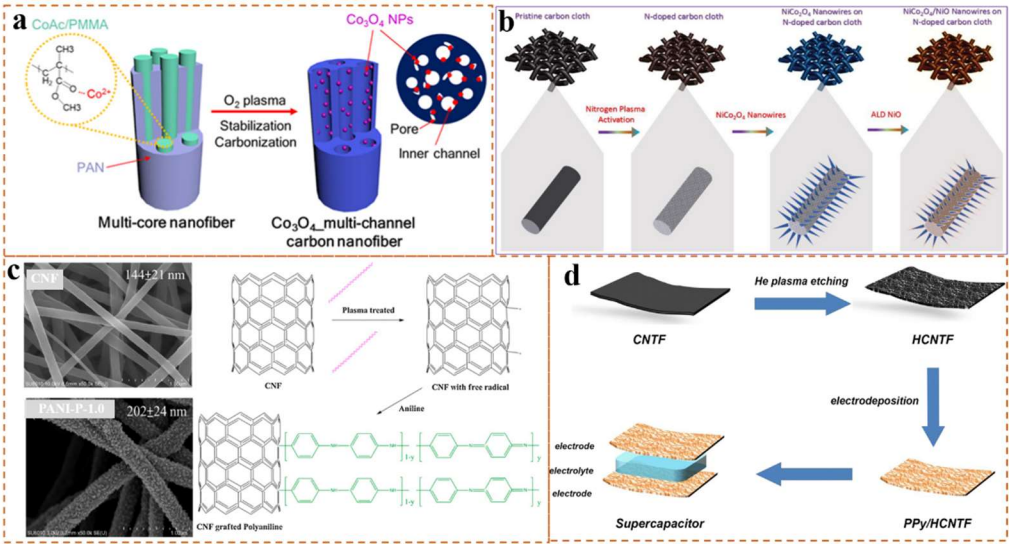

Figure 11. a) illustration of the synthesis of Co_3O_4-incorporated multichannel carbon nanofibers. Reproduced with permission [200], Copyright 2020, American Chemical Society. b) the schematic design to prepare the NCO/NiO core-shell nanowires arrays over the NCC substrate. Reproduced with permission [201], Copyright 2018, Wiley-VCH. c) Plasma induced polyaniline grafted on the CNFs, (the SEM images of CNFs and PANi-P-1.0). Reproduced with permission [204], Copyright 2016, Elsevier. d) the schematic diagrams of synthesis of PPy/HCNTF electrode and SC. Reproduced with permission [206], Copyright 2019, Springer.

Table 6. Summary of synthesis/modification of electrode materials in SCs by plasma technologies

Devices	Materials	Type of Plasma	Effects	Ref
SCs (Carbon materials)	Biochar with micro-meso-macropores structure	DBD plasma, O_2	Synthesis	[156]
	Biochar with micro-mesopores structure	Glow plasma, O_2		[157]
	Hierarchical	RF plasma, Ar-H_2-N_2		[158]

	cauliflower-like VGNs			
	CNTs	Glow plasma, O_2		[162]
	MWNTs	RF plasma, O_2		[163]
	Vertical graphene nanosheets (VGNs)	Microwave plasma, O_2	Introduce oxygen functional groups	[164]
	Graphene fibers	RF plasma, O_2		[165]
	Carbon nanofibers	RF plasma, O_2		[166]
	Graphene nanoribbons	DBD plasma, Ar	Obtain suitable oxygen functional groups	[169]
	N-doped CNTs	Glow plasma, Atmospheric		[170]
	N-doped rGO	Glow plasma, Atmospheric		[171]
	N-doped GO film	Glow plasma, N_2/H_2	N-doping	[172]
	N-doped graphite oxide	Glow plasma, N_2		[173]
	N-doped carbon cloth	Glow plasma, N_2		[174]
	N-doped graphene	RF plasma, N_2-O_2-CH_4		[175]
	N-doped carbon nanofibers	Glow plasma, Atmospheric		[176]
	B/N co-doped rGO	DBD plasma, H_2	B/N dual-doping	[180]
	N/S co-doped rGO	RF plasma, Ar-H_2	N/S dual-doping	[181]
	rGO with nanoporous structure	Glow plasma, Atmospheric	Morphological modulation	[184]
	Ni_2P, CoP and NiCoP nanoplates	Glow plasma, PH_3-He	Synthesis	[187]
SCs	HfN films	Glow plasma, Ar-Kr	Etching	[188]
(Pseudocapacitance materials)	Co_3O_4 powders	Microwave plasma, H_2	Introduce OVs	[191]
	Fe_2O_3	Glow plasma, PH_3-He	Introduce OVs	[192]
	MnO_2	Glow plasma, H_2 and O_2	Introduce lattice OVs	[193]
	$NiSe_2$ nanosheets	RF plasma, Ar	Introduce Se vacancies	[194]
SCs	Co_3O_4/CNFs	Glow plasma, O_2	Synthesis	[200]

(Carbon-based Composites)	$NiCo_2O_4$/NiO/N-doped carbon cloth	RF plasma, N_2		[201]
	SnO_2/CNTs	Glow plasma, Atmospheric		[202]
	Fe_2O_3/CNTs	Glow plasma, Atmospheric		[203]
	PANI/carbon nanofibers	RF plasma, Ar	Polymerization	[204]
	PANI/CNTs	RF plasma, Ar	Polymerization	[205]
	PPy/HCNTF	Glow plasma, He	Etching	[206]
	PPy/P-CNTs	RF plasma, Atmospheric	Introduce oxygen functional groups	[207]

4.2 Plasma Modification of Other Critical Materials

4.2.1 Separator

The separator is placed between the negative and positive electrodes, which play a key role in EES devices. Conventional polyolefin separators (*e.g.* polypropylene and polyethylene) have two main functions: high ion conductivity and electronic repulsion [208, 209]. However, the hydrophobic surfaces with low surface energy have poor wettability/holding ability to electrolyte solutions [210]. Therefore, it is urgent to develop separators materials with good wettability. The introduction of oxygen-containing functional groups through plasma is also an efficient method to improve the wettability of separator. For instance, Ahn *et al.* [211] employed the CO_2 plasma to modify the carbon-coated porous polypropylene (PP) separators. As shown in **Figure 12a**, the CO_2 plasma treatment generates -OH and -COOH on the surface of the carbon layer coated, which provide excellent wettability to the electrolyte, high Li^+ conductivity, and electrostatic repulsion toward negatively charged polysulfide ions. Meanwhile, the carbon layer can act as an upper current collector (electron path) that enhances the electrochemical utilization of S and reactivation of the trapped active material. Therefore, the Li-S batteries using the plasma-modified functional PP separators achieved much improved performance in terms of cyclability and reversible capacity even at high C-rates. In addition, polyethylene (PE) separators can also be decorated with oxygen-containing functional groups by the O_2 plasma [212] to improve the electrolyte wettability and retention of PE separators. The plasma-treated PE separator has enhanced compatibility with electrodes and reduced interfacial resistance. Therefore, the Li/$LiFePO_4$ cell assembled using the treated PE separator exhibited improved charge-discharge capability with lower interfacial resistance and more stable cycling performance as compared with that for the untreated separator. In addition, the plasma-induced grafting polymers is also an effective strategy to improve the wettability of separator. For example, the atmospheric plasma-induced grafting method is applied to PE separator for grafting polyampholyte [213], which make the separator more wettable with electrolyte. As shown in **Figure 12b**, when the net charge of the

polyampholyte is negative, attractive interactions between Li^+ and negative charges on separators can reduce the interfacial resistance of Li^+ transfer through the pores of PE separators, resulting in uniform Li^+ flux which helps to form stable SEI layer and improve capacity retention in the full cell tests. Herein, the summary of modification of separators by plasma technologies have also been presented in **Table 7**.

4.2.2 Current Collector

Metal substrate materials (*e.g.* Ni foam, Cu foam and Cu foil *etc.*) are used as current collector for EES devices due to their excellent electrical conductivity and stability. Using Li metal as an example, the current collector is the substrate for Li plating/stripping in practical electrochemical system, and its surface properties play an important role in the nucleation and growth of Li. Herein, the fabrication of lithiophilic surface through plasma technologies has been proven to induce uniform Li plating/stripping. One strategy is to decorate the surface of the current collector with lithiophilic metallic oxides (*e.g.* CuO). Luan *et al.* [214] applied N_2 plasma to treat CuO nanosheets grown on the Cu foil to synthesize N-doped porous CuO-decorated Cu foil. The CuO itself has excellent lithiophilicity, and it is easily to achieve N-doping and form porous structure in CuO nanosheets through N_2 plasma treatment, thus improving electrical conductivity and providing more bonding sites for Li nucleation. Therefore, the symmetric cell using the Li-plated electrode can be cycled for more than 600h with a low-voltage hysteresis (23.1 mV), which is much better than that of electrodes without plasma treatment. Another strategy is to *in-situ* form lithiophilic compounds (*e.g.* nitrides) on the surface of the current collector. As shown in **Figure 12c**, Zhu *et al.* [215] prepared a Ni_xN (x = 3, 4) layer on the Ni foam (NF) through N_2 plasma treatment, the Ni_xN decorated Ni foam (PNNF) exhibited high lithiophilicity owing to the Ni_xN and Li chemical reaction to form high ionic conductive Li_3N, leading to homogeneous Li deposition and effectively inhibiting the growth of Li dendrites. Therefore, the Li@PNNF half-cell exhibits lower nucleation overpotential in comparison to Li@NF half-cell. Moreover, the fabricated full-cell paired with $LiFePO_4$ cathode displayed a high reversible capacity 167.1 mA h/g after 300 cycles and stable cycling performance. In addition, *in-situ* formation of transition metal phosphides on the surface of the current collector through plasma technologies has been directly used as electrodes in EES devices. Specifically, the Ar/H_2 plasma activated phosphorus (P) vapor to allow efficient phosphorization of Cu foam without affecting the mechanical strength [216]. When P is deposited onto the Cu foam, it will be converted *in-situ* to Cu_3P by reacting with Cu (**Figure 12d**). The weight increase is due to the deposited P but the active material is Cu_3P. The obtained Cu_3P on Cu foam (Cu_3P/Cu) is free of any conductive additive and binder and can be directly used as the anode for LIBs. Cyclic voltammetry (CV) and *in-situ* XRD clearly revealed the behavior of the conversion reaction between Li^+ and Cu_3P, as evidenced by the reduction peak at 0.57V and 0.74V originating from the formation of Li rich Li_2CuP phase. As the voltage keeps decreasing, the reduction peak at ~0.05 V corresponds to the formation of amorphous Li_3P. Furthermore, the oxidation peaks at 0.86,1.14, 1.24 and 1.32V, which is attributed to the conversion from the Li rich Li_3P and Li_2CuP phase to the Cu_3P phase by the extraction of Li^+, indicated the reversible transformation between Cu_3P and Li^+. A high initial coulombic efficiency of >90% with the areal capacity up to 2.3 mA h/cm^2 after 50 cycles at 3.2 mA/cm^2 can be achieved. Herein, the summary of modification of current collectors by plasma technologies have also been presented in **Table 7**.

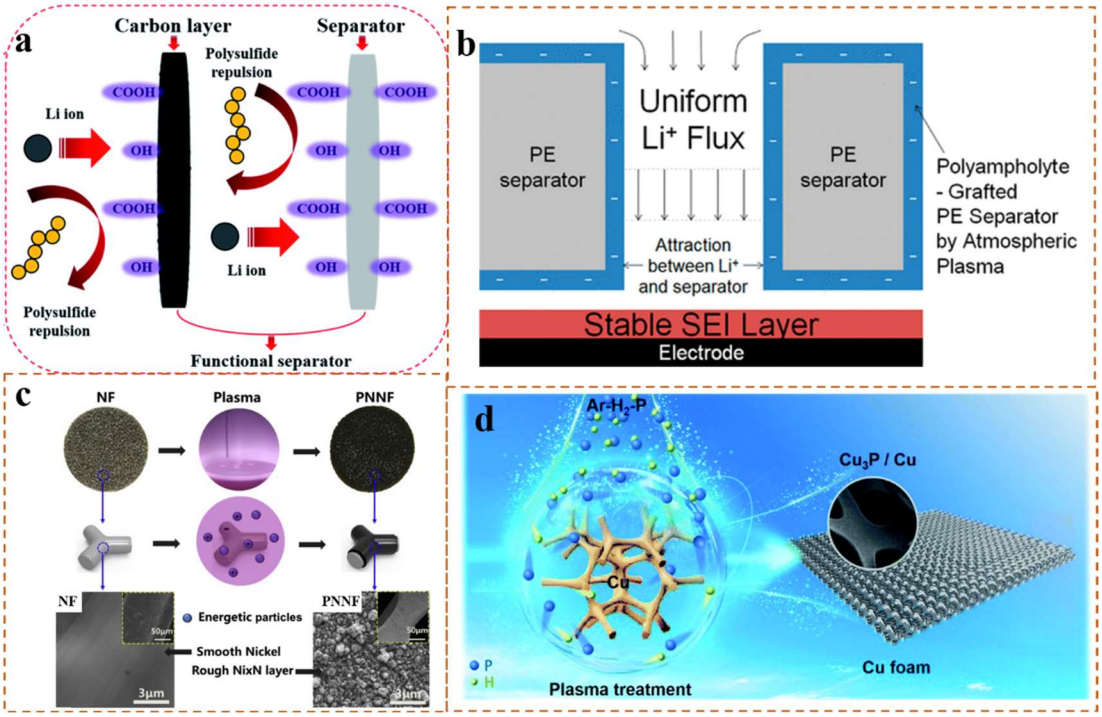

Figure 12. a) the schematic configuration of a carbon-coated functional separator modified by plasma. Reproduced with permission [211], Copyright 2019, Royal Society of Chemistry. b) the illustrative of Li^+ flux through pores of plasma-grafted polyampholyte PE separator, and the resulting SEI layers. Reproduced with permission [213], Copyright 2016, American Chemical Society. c) the schematics of the plasma nitriding process, and the SEM images of NF and PNNF. Reproduced with permission [215], Copyright 2019, Elsevier. d) the schematic of the synthesis of Cu_3P/Cu by exposing Cu foam in Ar-H_2 plasma. Reproduced with permission [216], Copyright 2020, Royal Society of Chemistry.

Table 7. Summary of modification of other critical materials by plasma technologies

Others	Materials	Type of Plasma	Effects	Ref
Separator	PP	RF plasma, CO_2	Introduce oxygen functional groups	[211]
	PE	RF plasma, O_2		[212]
	PE	RF plasma, Atmospheric	Grafting polymers	[213]
Current Collector	Cu foil	RF plasma, N_2	N-doping	[214]
	Ni foam	Glow plasma, N_2	Nitridation	[215]
	Cu foam	RF plasma, Ar-H_2	Phosphorization	[216]

5. Summary and Outlook

Plasma technologies have many attractive technological advantages over many other traditional materials processing and processes due to the complex discharge processes

that bring different combinations and states of active species (electron, ions, molecules *etc.*), leading to versatile physical and chemical reactions with solid surface such as exfoliation, deposition, etching, defects (doping/vacancy), surface functionalization and polymerization. Therefore, a huge amount of desirable phases, morphologies, or features of materials can be derived using the plasma-enabled approaches, and this provides enormous opportunities for multi-functionalization and property enhancement of advance materials and hence technological innovation in EES devices. Recent progress on LIBs, SIBs, PIBs, metal-based batteries, and SCs have been reviewed in this paper, the synthesis/modification of advance materials (*e.g.* electrode materials, separator, and current collector) by plasma technologies are discussed with corresponding examples. These examples are selected to demonstrate the applications of two major functions of plasma technologies in terms of material synthesis and surface modification. In the case of material synthesis, plasma technologies have the following common advantages: (1) high-speed collision between active species produces thermal effects inside the material, accelerating the growth rate of crystal materials; (2) the plasma synthesis process does not require harsh reaction conditions (*e.g.* high temperature), which can reduce the temperature of the reaction systems; (3) the nanoparticles in plasma are negatively charged, which avoids the aggregation of nanoparticles and obtains large specific surface area; (4) the electric field promotes the regular growth of particles to ensure uniform particle size; (5) the preparation of the composite materials via plasma-assisted methods (*e.g.* plasma-assisted milling) is highly controllable and efficient. In addition, there are several inherent advantages in plasma material surface modification: (1) plasma-enabled defect engineering (doping/vacancy) improves ion diffusion kinetics; (2) plasma-assisted *in-situ* oxidation/nitridation/sulfurization/phosphorization to prepare different components/functions surfaces; (3) plasma etching increases the surface roughness and specific surface area; (4) plasma introduces oxygen-containing functional groups (heteroatoms) to improve surface wettability due to increased active sites); (5) plasma grafting/polymerization introduces specific functional groups to improve surface wettability and chargeability; (6) plasma-assisted deposition/pyrolysis processes to prepare the surface coating layers (*e.g.* carbon coating). Of course, the physical and chemical changes are closely related in the actual plasma process, and the electrochemical performance improvement could be attributed to both physical and chemical change or the synergy of them.

Despite the promising achievements to date, there are still some challenges that need to be addressed in the future to realize the full potential of plasma-based strategies:

i. The in-depth studies on the interaction mechanisms between plasma and materials to advance scientific understanding and provide new insights for technological innovation. At present, the theoretic analysis of most research papers mainly relies on the existing material-plasma interaction theory that has been developed based upon large bulk materials. However, the EES materials often exist in the form of nano/micro sized materials with various compositions (van der Waals force, hydrogen bond, metallic bond, ionic bond, or covalent bond) and structures (particle, porous, layer, core-shell, *etc.*). Moreover, the as-mentioned plasma can be produced by various discharge modes, leading to different characteristic properties (energy density, ion/electron temperature, ion/electron concentration) by modulating the operating parameters (gases, power, time, and frequency *etc.*). However, the material-plasma interaction mechanisms are far from being fully understood due to the combined effect of multiple species (*e.g.* ions, electrons, radicals, excited neutrals and photons) in the plasma environment. A key

challenge for this complex and dynamic environment is how to achieve desirable surface reactions to meet the specific requirements with precise control, which requires a better understanding of the role of the incident species fluxes, species energy dependence and species selectivity. Therefore, plasma diagnostics and modelling should be employed during the plasma-enhanced synthesis and modification to establish the relationship between plasma species and the performance improvement. Furthermore, there is still a general challenge of producing 2D electrode materials with high purity and crystallinity. This may be a significant opportunity for plasma research, not only limited to the synthesis of graphene but also other promising 2D materials, such as transition metal chalcogenides (M_aX_b, M =Ti, V, Mo, etc. X = S, Se, Te, etc.). Hence, the in-depth fundamental studies on the material-plasma interaction theory for the EES materials are necessary.

ii. The investigation into the relationship between plasma treatment and the formation of defect/phase/morphology as well as the electrochemical performance of EES materials. Aforementioned, the plasma can produce versatile physical and chemical effects, such as deposition, exfoliation, vacancy, doping, etching, functionalization, reduction and polymerization. However, the knowledge of the capability, limits and specificity of the plasma-derived materials are limited. For example, defect engineering (vacancy/heteroatom) is an important strategy to enhance the electronic and ion conductivity of electrode materials, thus improving the charge transfer process and electrochemical reaction rate, the efficiency of defects activation has been found to be highly variable, necessitating a much better understanding of the physical mechanisms governing defects in plasma-derived materials. To address this challenge, understanding the characteristics of the defects introduced by plasma and their effects on the electrochemical properties can provide the theoretical guidance for research, it is necessary to combine the computational modelling, plasma diagnostics and advanced characterization techniques (*e.g. in-situ* measurements) to explore the relationship of plasma treatment, material characteristics and electrochemical performance.

iii. The diversification of the development and application of plasma technologies. Firstly, the existing plasma technologies suitable for the EES materials are limited. It is important to further explore and develop targeted plasma devices and novel processes. Meanwhile, the controllability, economy, and energy efficiency of plasma technologies also need to be considered. Secondary, as an enabling technology, it is believed that the plasma is a powerful and universe tool to almost all electrode materials, and other key materials in EES devices, such as separators and current collectors, where surface properties are also very important.

iv. There is no doubt that plasma technologies can synthesize or modify various components of EES systems with even superior performance compared to conventional methods. Still, if plasma technologies are applied to the EES device manufacturing market, they will have to adapt to existing assembly lines. The challenges in this case are the production scale-up and quality control. For example, moving from vacuum to atmospheric conditions increases the plasma density and the production rate, but it comes with gas heating and less selectivity, and the electron temperature and nucleated nanoparticle temperature are critical parameters to follow to obtain the desired crystalline phase, especially for complex layered oxides. Furthermore, for binder-free electrodes, flexible coatings and thin films will have to be deposited onto the current collector with better consistency, which may not be directly compatible with existing assembly lines.

Finally, we hope that readers can systematically understand the mechanism of synthesis or modification of EES materials by plasma technology and realize that plasma-enabled materials science is an interesting and fruitful field. Meanwhile, we also hope readers to join this rapidly developing field, and suggest more efficient strategies to further promote the applications of plasma-enabled materials in various fields, including but not limited to electrochemical energy storage.

Acknowledgements

The authors would like to thank the financial supports from the MOST (2019YFE0191500), the Natural Science Foundation of Jiangsu Province of China (BK20211172) and the Fundamental Research Funds for the Central Universities. The author Zhen Wang also appreciates his wife, Yongxia Zhang, for continuous encouragement, accompany and support.

Conflict of Interest

The authors declare no conflict of interest.

References

[1] B. Bayatsarmadi, Y. Zheng, A. Vasileff, S.-Z. Qiao, Recent Advances in Atomic Metal Doping of Carbon-based Nanomaterials for Energy Conversion, Small 13(21) (2017) 1700191. https://doi.org/10.1002/smll.201700191.

[2] D.U. Lee, P. Xu, Z.P. Cano, A.G. Kashkooli, M.G. Park, Z. Chen, Recent progress and perspectives on bi-functional oxygen electrocatalysts for advanced rechargeable metal-air batteries, Journal of Materials Chemistry A 4(19) (2016) 7107-7134. https://doi.org/10.1039/c6ta00173d.

[3] X. Li, S. Zheng, L. Jin, Y. Li, P. Geng, H. Xue, H. Pang, Q. Xu, Metal-Organic Framework-Derived Carbons for Battery Applications, Advanced Energy Materials 8(23) (2018) 1800716. https://doi.org/10.1002/aenm.201800716.

[4] S. Dou, L. Tao, R. Wang, S. El Hankari, R. Chen, S. Wang, Plasma-Assisted Synthesis and Surface Modification of Electrode Materials for Renewable Energy, Advanced Materials 30(21) (2018) 1705850. https://doi.org/10.1002/adma.201705850.

[5] C.-J. Liu, J. Zou, K. Yu, D. Cheng, Y. Han, J. Zhan, C. Ratanatawanate, B.W.L. Jang, Plasma application for more environmentally friendly catalyst preparation, Pure and Applied Chemistry 78(6) (2006) 1227-1238. https://doi.org/10.1351/pac200678061227.

[6] A. Bogaerts, E.C. Neyts, Plasma technology: an emerging technology for energy storage, ACS Energy Letters 3(4) (2018) 1013-1027. https://doi.org/10.1021/acsenergylett.8b00184.

[7] J. Li, X. Jing, Q. Li, S. Li, X. Gao, X. Feng, B. Wang, Bulk COFs and COF nanosheets for electrochemical energy storage and conversion, Chemical Society Reviews 49(11) (2020) 3565-3604. https://doi.org/10.1039/d0cs00017e.

[8] D. Wang, Y. Zou, L. Tao, Y. Zhang, Z. Liu, S. Du, S. Zang, S. Wang, Low-temperature plasma technology for electrocatalysis, Chinese Chemical Letters 30(4) (2019) 826-838. https://doi.org/10.1016/j.cclet.2019.03.051.

[9] B. Ouyang, Y. Zhang, X. Xia, R.S. Rawat, H.J. Fan, A brief review on plasma for synthesis and processing of electrode materials, Materials Today Nano 3 (2018) 28-47. https://doi.org/10.1016/j.mtnano.2018.11.002.

[10] H. Liang, F. Ming, H.N. Alshareef, Applications of Plasma in Energy Conversion and Storage Materials, Advanced Energy Materials 8(29) (2018) 1801804. https://doi.org/10.1002/aenm.201801804.

[11] Y. Zhang, R.S. Rawat, H.J. Fan, Plasma for Rapid Conversion Reactions and Surface Modification of Electrode Materials, Small Methods 1(9) (2017) 1700164. https://doi.org/10.1002/smtd.201700164.

[12] J. Joseph, A.T. Murdock, D.H. Seo, Z.J. Han, A.P. O'Mullane, K. Ostrikov, Plasma Enabled

Synthesis and Processing of Materials for Lithium-Ion Batteries, Advanced Materials Technologies 3(9) (2018) 1800070. https://doi.org/10.1002/admt.201800070.

[13] Q. Chen, J. Li, Y. Li, A review of plasma-liquid interactions for nanomaterial synthesis, Journal of Physics D-Applied Physics 48(42) (2015) 424005. https://doi.org/10.1088/0022-3727/48/42/424005.

[14] L. Tonks, I. Langmuir, Oscillations in ionized gases, Physical Review 33(2) (1929) 195-210. https://doi.org/10.1103/PhysRev.33.195.

[15] R. Fitzpatrick, Plasma Physics, CRC Press2014.

[16] F. Romanelli, Plasma Physics and Engineering, Second Edition, CRC Press2011.

[17] D.A. Gurnett, A. Bhattacharjee, Introduction to Plasma Physics, Second Edition, Cambridge University Press2014.

[18] S. Duan, X. Liu, Y. Wang, Y. Meng, A. Alsaedi, T. Hayat, J. Li, Plasma surface modification of materials and their entrapment of water contaminant: A review, Plasma Processes and Polymers 14(9) (2017) e1600218. https://doi.org/10.1002/ppap.201600218.

[19] G. Petitpas, J.D. Rollier, A. Darmon, J. Gonzalez-Aguilar, R. Metkemeijer, L. Fulcheri, A comparative study of non-thermal plasma assisted reforming technologies, International Journal of Hydrogen Energy 32(14) (2007) 2848-2867. https://doi.org/10.1016/j.ijhydene.2007.03.026.

[20] R. Foest, M. Schmidt, K. Becker, Microplasmas, an emerging field of low-temperature plasma science and technology, International Journal of Mass Spectrometry 248(3) (2006) 87-102. https://doi.org/10.1016/j.ijms.2005.11.010.

[21] U. Kogelschatz, B. Eliasson, W. Egli, From ozone generators to flat television screens: history and future potential of dielectric-barrier discharges, Pure and Applied Chemistry 71(10) (1999) 1819-1828. https://doi.org/10.1351/pac199971101819.

[22] H. Heidsieck, Status of vacuum and plasma technology, Surface & Coatings Technology 112(1-3) (1999) 324-338. https://doi.org/10.1016/s0257-8972(98)00767-1.

[23] H.H. Kim, Nonthermal plasma processing for air-pollution control: A historical review, current issues, and future prospects, Plasma Processes and Polymers 1(2) (2004) 91-110. https://doi.org/10.1002/ppap.200400028.

[24] R. Morrish, T. Haak, C.A. Wolden, Low-Temperature Synthesis of n-Type WS_2 Thin Films via H_2S Plasma Sulfurization of WO_3, Chemistry of Materials 26(13) (2014) 3986-3992. https://doi.org/10.1021/cm501566h.

[25] H. Liang, A.N. Gandi, D.H. Anjum, X. Wang, U. Schwingenschlogl, H.N. Alshareef, Plasma-Assisted Synthesis of NiCoP for Efficient Overall Water Splitting, Nano Letters 16(12) (2016) 7718-7725. https://doi.org/10.1021/acs.nanolett.6b03803.

[26] J. Musil, P. Baroch, Discharge in dual magnetron sputtering system, IEEE Transactions on Plasma Science 33(2) (2005) 338-339. https://doi.org/10.1109/tps.2005.844996.

[27] Z. Wu, Y. Zhao, W. Jin, B. Jia, J. Wang, T. Ma, Recent Progress of Vacancy Engineering for Electrochemical Energy Conversion Related Applications, Advanced Functional Materials 31(9) (2021) 2009070. https://doi.org/10.1002/adfm.202009070.

[28] X. Wang, G. Sun, P. Routh, D.-H. Kim, W. Huang, P. Chen, Heteroatom-doped graphene materials: syntheses, properties and applications, Chemical Society Reviews 43(20) (2014) 7067-7098. https://doi.org/10.1039/c4cs00141a.

[29] Y. Li, M. Chen, B. Liu, Y. Zhang, X. Liang, X. Xia, Heteroatom Doping: An Effective Way to Boost Sodium Ion Storage, Advanced Energy Materials 10(27) (2020) 2000927. https://doi.org/10.1002/aenm.202000927.

[30] L. Shao, E. Xie, Y. Lu, D. He, G. Chen, Field Electron Emission of N-Doped Diamond Films by Growth-Doping and Ion Implantation, Chinese Journal of Semiconductors 20 (1999) 785-790. https://doi.org/10.1109/ISIC.1999.796628.

[31] S. Banerjee, E. Adhikari, P. Sapkota, A. Sebastian, S. Ptasinska, Atmospheric Pressure Plasma Deposition of TiO_2: A Review, Materials 13(13) (2020) 2931. https://doi.org/10.3390/ma13132931.

[32] V.M. Donnelly, A. Kornblit, Plasma etching: Yesterday, today, and tomorrow, Journal of Vacuum

Science & Technology A 31(5) (2013) 050825. https://doi.org/10.1116/1.4819316.

[33] J.C. Tinoco, M. Estrada, H. Baez, A. Cerdeira, Room temperature plasma oxidation: A new process for preparation of ultrathin layers of silicon oxide, and high dielectric constant materials, Thin Solid Films 496(2) (2006) 546-554. https://doi.org/10.1016/j.tsf.2005.08.351.

[34] B. Ouyang, Y. Zhang, Z. Zhang, H.J. Fan, R.S. Rawat, Nitrogen-Plasma-Activated Hierarchical Nickel Nitride Nanocorals for Energy Applications, Small 13(34) (2017) 1604265. https://doi.org/10.1002/smll.201604265.

[35] R. Morrish, R. Silverstein, C.A. Wolden, Synthesis of Stoichiometric FeS_2 through Plasma-Assisted Sulfurization of Fe_2O_3 Nanorods, Journal of the American Chemical Society 134(43) (2012) 17854-17857. https://doi.org/10.1021/ja307412e.

[36] Y. Shi, B. Zhang, Recent advances in transition metal phosphide nanomaterials: synthesis and applications in hydrogen evolution reaction, Chemical Society Reviews 45(6) (2016) 1529-1541. https://doi.org/10.1039/c5cs00434a.

[37] J. Lee, T.S. Williams, R.F. Hicks, Atmospheric pressure plasma reduction of copper oxide to copper metal, Journal of Vacuum Science & Technology A 39(2) (2021) 023001. https://doi.org/10.1116/6.0000704.

[38] J. Chen, X. Shi, S. Qi, M. Mohai, I. Bertoti, Y. Gao, H. Dong, Reducing and Multiple-element Doping of Graphene Oxide Using Active Screen Plasma Treatments, Carbon 95 (2015) 338-346. https://doi.org/10.1016/j.carbon.2015.08.046.

[39] J. Friedrich, Mechanisms of Plasma Polymerization-Reviewed from a Chemical Point of View, Plasma Processes and Polymers 8(9) (2011) 783-802. https://doi.org/10.1002/ppap.201100038.

[40] R. Srinivasan, P.A. Demirev, B.G. Carkhuff, S. Santhanagopalan, J.A. Jeevarajan, T.P. Barrera, Review-Thermal Safety Management in Li-Ion Batteries: Current Issues and Perspectives, Journal of the Electrochemical Society 167(14) (2020) 140516. https://doi.org/10.1149/1945-7111/abc0a5.

[41] K.N. Wood, M. Noked, N.P. Dasgupta, Lithium Metal Anodes: Toward an Improved Understanding of Coupled Morphological, Electrochemical, and Mechanical Behavior, ACS Energy Letters 2(3) (2017) 664-672. https://doi.org/10.1021/acsenergylett.6b00650.

[42] M. Rosa Palacin, Recent advances in rechargeable battery materials: a chemist's perspective, Chemical Society Reviews 38(9) (2009) 2565-2575. https://doi.org/10.1039/b820555h.

[43] M.-S. Balogun, W. Qiu, Y. Luo, H. Meng, W. Mai, A. Onasanya, T.K. Olaniyi, Y. Tong, A review of the development of full cell lithium-ion batteries: The impact of nanostructured anode materials, Nano Research 9(10) (2016) 2823-2851. https://doi.org/10.1007/s12274-016-1171-1.

[44] K.-T. Kim, G. Ali, K.Y. Chung, C.S. Yoon, H. Yashiro, Y.-K. Sun, J. Lu, K. Amine, S.-T. Myung, Anatase Titania Nanorods as an Intercalation Anode Material for Rechargeable Sodium Batteries, Nano Letters 14(2) (2014) 416-422. https://doi.org/10.1021/nl402747x.

[45] R. Ata Ur, G. Ali, A. Badshah, K.Y. Chung, K.-W. Nam, M. Jawad, M. Arshad, S.M. Abbas, Superior shuttling of lithium and sodium ions in manganese-doped titania @ functionalized multiwall carbon nanotube anodes, Nanoscale 9(28) (2017) 9859-9871. https://doi.org/10.1039/c7nr01417a.

[46] S. Sun, D. Chen, M. Shen, L. Qin, Z. Wang, Y. Wu, J. Chen, Plasma modulated MOF-derived TiO_2/C for enhanced lithium storage, Chemical Engineering Journal 417 (2021) 128003. https://doi.org/10.1016/j.cej.2020.128003.

[47] X. Li, J. Zhao, S. Sun, L. Huang, Z. Qiu, P. Dong, Y. Zhang, The application of plasma treatment for Ti^{3+} modified TiO_2 nanowires film electrode with enhanced lithium-storage properties, Electrochimica Acta 211 (2016) 395-403. https://doi.org/10.1016/j.electacta.2016.05.192.

[48] L. Shen, E. Uchaker, X. Zhang, G. Cao, Hydrogenated $Li_4Ti_5O_{12}$ Nanowire Arrays for High Rate Lithium Ion Batteries, Advanced Materials 24(48) (2012) 6502-6506. https://doi.org/10.1002/adma.201203151.

[49] C.Y. Ouyang, Z.Y. Zhong, M.S. Lei, Ab initio studies of structural and electronic properties of $Li_4Ti_5O_{12}$ spinel, Electrochemistry Communications 9(5) (2007) 1107-1112. https://doi.org/10.1016/j.elecom.2007.01.013.

[50] C.-K. Lan, S.-I. Chuang, Q. Bao, Y.-T. Liao, J.-G. Duh, One-step argon/nitrogen binary plasma jet

irradiation of $Li_4Ti_5O_{12}$ for stable high-rate lithium ion battery anodes, Journal of Power Sources 275 (2015) 660-667. https://doi.org/10.1016/j.jpowsour.2014.11.074.

[51] J. Zhu, J. Chen, H. Xu, S. Sun, Y. Xu, M. Zhou, X. Gao, Z. Sun, Plasma-Introduced Oxygen Defects Confined in $Li_4Ti_5O_{12}$ Nanosheets for Boosting Lithium-Ion Diffusion, ACS Applied Materials & Interfaces 11(19) (2019) 17384-17392. https://doi.org/10.1021/acsami.9b02102.

[52] S. Sun, Y. Wu, J. Zhu, C. Lu, Y. Sun, Z. Wang, J. Chen, Stabilizing plasma-induced highly nitrogen-deficient g-C_3N_4 by heteroatom-refilling for excellent lithium-ion battery anodes, Chemical Engineering Journal 427 (2022) 131032. https://doi.org/10.1016/j.cej.2021.131032.

[53] M.M. Thackeray, J.T. Vaughey, C.S. Johnson, A.J. Kropf, R. Benedek, L.M.L. Fransson, K. Edstrom, Structural considerations of intermetallic electrodes for lithium batteries, Journal of Power Sources 113(1) (2003) 124-130. https://doi.org/10.1016/s0378-7753(02)00538-4.

[54] D. Larcher, S. Beattie, M. Morcrette, K. Edstroem, J.-C. Jumas, J.-M. Tarascon, Recent findings and prospects in the field of pure metals as negative electrodes for Li-ion batteries, Journal of Materials Chemistry 17(36) (2007) 3759-3772. https://doi.org/10.1039/b705421c.

[55] K. Puhakainen, M. Bostrom, T.L. Groy, U. Haeussermann, A new phase in the system lithium-aluminum: Characterization of orthorhombic Li_2Al, Journal of Solid State Chemistry 183(11) (2010) 2528-2533. https://doi.org/10.1016/j.jssc.2010.08.029.

[56] X. Chang, Z. Xie, Z. Liu, X. Zheng, J. Zheng, X. Li, Enabling High Performance Lithium Storage in Aluminum: The Double Edged Surface Oxide, Nano Energy 41 (2017) 731-737. https://doi.org/10.1016/j.nanoen.2017.10.017.

[57] X. Chang, Z. Xie, Z. Liu, X. Zheng, J. Zheng, X. Li, Aluminum: An underappreciated anode material for lithium-ion batteries, Energy Storage Materials 25 (2020) 93-99. https://doi.org/10.1016/j.ensm.2019.10.027.

[58] X. Zuo, J. Zhu, P. Mueller-Buschbaum, Y.-J. Cheng, Silicon based lithium-ion battery anodes: A chronicle perspective review, Nano Energy 31 (2017) 113-143. https://doi.org/10.1016/j.nanoen.2016.11.013.

[59] L.Y. Beaulieu, K.W. Eberman, R.L. Turner, L.J. Krause, J.R. Dahn, Colossal reversible volume changes in lithium alloys, Electrochemical and Solid State Letters 4(9) (2001) A137-A140. https://doi.org/10.1149/1.1388178.

[60] E. Park, H. Yoo, J. Lee, M.-S. Park, Y.-J. Kim, H. Kim, Dual-Size Silicon Nanocrystal-Embedded SiO_x Nanocomposite as a High-Capacity Lithium Storage Material, ACS Nano 9(7) (2015) 7690-7696. https://doi.org/10.1021/acsnano.5b03166.

[61] H. Wu, G. Chan, J.W. Choi, I. Ryu, Y. Yao, M.T. McDowell, S.W. Lee, A. Jackson, Y. Yang, L. Hu, Y. Cui, Stable Cycling of Double-Walled Silicon Nanotube Battery Anodes Through Solid-Electrolyte Interphase Control, Nature Nanotechnology 7(5) (2012) 309-314. https://doi.org/10.1038/nnano.2012.35.

[62] J. Hu, L. Fu, R. Rajagopalan, Q. Zhang, J. Luan, H. Zhang, Y. Tang, Z. Peng, H. Wang, Nitrogen Plasma-Treated Core-Bishell $Si@SiO_x@TiO_{2\text{-delta}}$: Nanoparticles with Significantly Improved Lithium Storage Performance, ACS Applied Materials & Interfaces 11(31) (2019) 27658-27666. https://doi.org/10.1021/acsami.9b04415.

[63] Y. Tang, J. Chen, Z. Mao, D. Wang, Facile fabrication of oxide layer for si anode with enhanced lithium storage performances via plasma oxidation, Journal of Materials Science-Materials in Electronics 32(2) (2021) 2158-2171. https://doi.org/10.1007/s10854-020-04981-5.

[64] H. Kong, C. Yan, C. Lv, J. Pei, G. Chen, Electric field effect in a Co_3O_4/TiO_2 p-n junction for superior lithium-ion storage, Materials Chemistry Frontiers 3(5) (2019) 909-915. https://doi.org/10.1039/c9qm00007k.

[65] F. Wu, M. Wang, Y. Su, S. Chen, B. Xu, Effect of TiO_2-coating on the electrochemical performances of $LiCo_{1/3}Ni_{1/3}Mn_{1/3}O_2$, Journal of Power Sources 191(2) (2009) 628-632. https://doi.org/10.1016/j.jpowsour.2009.02.063.

[66] D.-H. Wang, L. Jia, X.-L. Wu, L.-Q. Lu, A.-W. Xu, One-Step Hydrothermal Synthesis of N-doped TiO_2/C Nanocomposites with High Visible Light Photocatalytic Activity, Nanoscale 4(2) (2012) 576-584. https://doi.org/10.1039/c1nr11353d.

[67] H.-S. Tsai, C.-H. Hsu, C.-C. Chi, Y.-C. Wang, F.-W. Liu, S.-Y. Tang, C.-J. Tsai, H. Ouyang, Y.-L. Chueh, J.-H. Liang, Non-layered Ti_2N synthesized by plasma process for the anodes of lithium-ion batteries, Inorganic Chemistry Frontiers 6(1) (2019) 172-175. https://doi.org/10.1039/c8qi01105b.

[68] G. Du, Z. Guo, S. Wang, R. Zeng, Z. Chen, H. Liu, Superior stability and high capacity of restacked molybdenum disulfide as anode material for lithium ion batteries, Chemical Communications 46(7) (2010) 1106-1108. https://doi.org/10.1039/b920277c.

[69] X. Fan, Y. Shi, L. Gou, D. Li, Electrodeposition of Three-Dimensional Macro-/Mesoporous Co_3O_4 Nanosheet Arrays as for Ultrahigh Rate Lithium-ion Battery, Electrochimica Acta 142 (2014) 268-275. https://doi.org/10.1016/j.electacta.2014.08.003.

[70] L. Zhan, S. Wang, L.-X. Ding, Z. Li, H. Wang, Grass-like Co_3O_4 Nanowire Arrays Anode with High Rate Capability and Excellent Cycling Stability for Lithium-ion Batteries, Electrochimica Acta 135 (2014) 35-41. https://doi.org/10.1016/j.electacta.2014.04.139.

[71] H. Long, M. Zhang, Q. Wang, L. Xing, S. Wang, X. Xue, Plasma-treated Co_3O_4/Graphene Nanocomposite as High Performance Anode of Lithium-ion Battery, Journal of Alloys and Compounds 701 (2017) 200-207. https://doi.org/10.1016/j.jallcom.2017.01.108.

[72] Y. Liu, L. Zhang, H. Wang, C. Yu, X. Yan, Q. Liu, B. Xu, L.-m. Wang, Synthesis of severe lattice distorted MoS_2 coupled with hetero-bonds as anode for superior lithium-ion batteries, Electrochimica Acta 262 (2018) 162-172. https://doi.org/10.1016/j.electacta.2018.01.023.

[73] Y. Liu, L. Zhang, Y. Zhao, T. Shen, X. Yan, C. Yu, H. Wang, H. Zeng, Novel plasma-engineered MoS_2 nanosheets for superior lithium-ion batteries, Journal of Alloys and Compounds 787 (2019) 996-1003. https://doi.org/10.1016/j.jallcom.2019.02.156.

[74] A.J. S, The kinetics and mechanism of solid-state spinel formation-A review and critique, Oxidation of Metals 1(2) (1969) 171-198.

[75] A. Manthiram, A reflection on lithium-ion battery cathode chemistry, Nature Communications 11(1) (2020) 1550. https://doi.org/10.1038/s41467-020-15355-0.

[76] K. Zhang, J.-T. Lee, P. Li, B. Kang, J.H. Kim, G.-R. Yi, J.H. Park, Conformal Coating Strategy Comprising N-doped Carbon and Conventional Graphene for Achieving Ultrahigh Power and Cyclability of $LiFePO_4$, Nano Letters 15(10) (2015) 6756-6763. https://doi.org/10.1021/acs.nanolett.5b02604.

[77] C. Gong, Z. Xue, S. Wen, Y. Ye, X. Xie, Advanced carbon materials/olivine $LiFePO_4$ composites cathode for lithium ion batteries, Journal of Power Sources 318 (2016) 93-112. https://doi.org/10.1016/j.jpowsour.2016.04.008.

[78] X. Tian, W. Chen, Z. Jiang, Z.-J. Jiang, Porous carbon-coated $LiFePO_4$ nanocrystals prepared by in situ plasma-assisted pyrolysis as superior cathode materials for lithium ion batteries, Ionics 26(6) (2020) 2715-2726. https://doi.org/10.1007/s11581-019-03422-6.

[79] Z. Jiang, B. Zhang, Q. Shen, Z.-J. Jiang, In-situ plasma assisted formation of graphitic nanosheet supported N-doped carbon-coated antisite defectless $LiFePO_4$ as a high-performance cathode material for lithium-ion batteries, Journal of Alloys and Compounds 806 (2019) 864-873. https://doi.org/10.1016/j.jallcom.2019.07.309.

[80] B.P. Ajayi, A.K. Thapa, U. Cvelbar, J.B. Jasinski, M.K. Sunkara, Atmospheric plasma spray pyrolysis of lithiated nickel-manganese-cobalt oxides for cathodes in lithium ion batteries, Chemical Engineering Science 174 (2017) 302-310. https://doi.org/10.1016/j.ces.2017.09.022.

[81] G. Zhu, K. Wen, W. Lv, X. Zhou, Y. Liang, F. Yang, Z. Chen, M. Zou, J. Li, Y. Zhang, W. He, Materials insights into low-temperature performances of lithium-ion batteries, Journal of Power Sources 300 (2015) 29-40. https://doi.org/10.1016/j.jpowsour.2015.09.056.

[82] X. Li, W. He, L. Chen, W. Guo, J. Chen, Z. Xiao, Hydrothermal synthesis and electrochemical performance studies of Al_2O_3-coated $LiNi_{1/3}Co_{1/3}Mn_{1/3}O_2$ for lithium-ion batteries, Ionics 20(6) (2014) 833-840. https://doi.org/10.1007/s11581-013-1041-8.

[83] Q. Jiang, X. Wang, Y. Zhang, N. Yuan, J. Tang, High Efficient and Environment Friendly Plasma-Enhanced Synthesis of Al_2O_3-Coated $LiNi_{1/3}Co_{1/3}Mn_{1/3}O_2$ With Excellent Electrochemical Performance, Frontiers in Chemistry 8 (2020) 72. https://doi.org/10.3389/fchem.2020.00072.

[84] Z. Chen, Y. Liu, Z. Lu, R. Hu, J. Cui, H. Xu, Y. Ouyang, Y. Zhang, M. Zhu, Plasma-assisted Coating

of Nanosized SnO_2 on $LiNi_{0.5}Co_{0.2}Mn_{0.3}O_2$ Cathodes for Enhanced Cyclic Stability of Lithium-ion Batteries, Journal of Alloys and Compounds 803 (2019) 71-79. https://doi.org/10.1016/j.jallcom.2019.06.281.

[85] H.M. Wu, J.P. Tu, Y.F. Yuan, X.T. Chen, J.Y. Xiang, X.B. Zhao, G.S. Cao, One-step Synthesis $LiMn_2O_4$ Cathode by a Hydrothermal Method, Journal of Power Sources 161(2) (2006) 1260-1263. https://doi.org/10.1016/j.jpowsour.2006.05.011.

[86] H.W. Chan, J.G. Duh, S.R. Sheen, $LiMn_2O_4$ cathode doped with excess lithium and synthesized by co-precipitation for Li-ion batteries, Journal of Power Sources 115(1) (2003) 110-118. https://doi.org/10.1016/s0378-7753(02)00616-x.

[87] Q. Jiang, X. Wang, Z. Tang, Improving the Electrochemical Performance of $LiMn_2O_4$ by Amorphous Carbon Coating, Fullerenes Nanotubes and Carbon Nanostructures 23(8) (2015) 676-679. https://doi.org/10.1080/1536383x.2014.952369.

[88] Q. Jiang, H. Zhang, S. Wang, Plasma-enhanced low-temperature solid-state synthesis of spinel $LiMn_2O_4$ with superior performance for lithium-ion batteries, Green Chemistry 18(3) (2016) 662-666. https://doi.org/10.1039/c5gc01563d.

[89] J.B. Goodenough, Cathode materials: A personal perspective, Journal of Power Sources 174(2) (2007) 996-1000. https://doi.org/10.1016/j.jpowsour.2007.06.217.

[90] Q. Jiang, D. Liu, H. Zhang, S. Wang, Plasma-Assisted Sulfur Doping of $LiMn_2O_4$ for High-Performance Lithium-Ion Batteries, Journal of Physical Chemistry C 119(52) (2015) 28776-28782. https://doi.org/10.1021/acs.jpcc.5b10298.

[91] Y. Yang, J. Wang, C. Wang, R. Guan, D. Lu, S. Zhao, S. Liu, X. Bian, Solvent-free synthesis of morphology-controllable nickel sulfides via one-pot plasma reactions for high-performance lithium-ion batteries, Green Chemistry 22(21) (2020) 7460-7467. https://doi.org/10.1039/d0gc02208j.

[92] N.A. Chernova, M. Roppolo, A.C. Dillon, M.S. Whittingham, Layered vanadium and molybdenum oxides: batteries and electrochromics, Journal of Materials Chemistry 19(17) (2009) 2526-2552. https://doi.org/10.1039/b819629j.

[93] Y. Iriyama, T. Abe, M. Inaba, Z. Ogumi, Transmission electron microscopy (TEM) analysis of two-phase reaction in electrochemical lithium insertion within alpha-MoO_3, Solid State Ionics 135(1-4) (2000) 95-100. https://doi.org/10.1016/s0167-2738(00)00338-6.

[94] D. Larcher, J.M. Tarascon, Towards greener and more sustainable batteries for electrical energy storage, Nature Chemistry 7(1) (2015) 19-29. https://doi.org/10.1038/nchem.2085.

[95] G. Zhang, T. Xiong, M. Yan, L. He, X. Liao, C. He, C. Yin, H. Zhang, L. Mai, alpha-MoO_{3-x} by plasma etching with improved capacity and stabilized structure for lithium storage, Nano Energy 49 (2018) 555-563. https://doi.org/10.1016/j.nanoen.2018.04.075.

[96] N. Mahmood, Y. Hou, Electrode Nanostructures in Lithium-Based Batteries, Advanced Science 1(1) (2014) 1400012. https://doi.org/10.1002/advs.201400012.

[97] W. Zhang, Y. Liu, Z. Guo, Approaching high-performance potassium-ion batteries via advanced design strategies and engineering, Science Advances 5(5) (2019) eaav7412. https://doi.org/10.1126/sciadv.aav7412.

[98] S. Wu, W. Wang, M. Li, L. Cao, F. Lyu, M. Yang, Z. Wang, Y. Shi, B. Nan, S. Yu, Z. Sun, Y. Liu, Z. Lu, Highly durable organic electrode for sodium-ion batteries via a stabilized alpha-C radical intermediate, Nature Communications 7 (2016) 13318. https://doi.org/10.1038/ncomms13318.

[99] E. Castillo-Martinez, J. Carretero-Gonzalez, M. Armand, Polymeric Schiff Bases as Low-Voltage Redox Centers for Sodium-Ion Batteries, Angewandte Chemie-International Edition 53(21) (2014) 5341-5345. https://doi.org/10.1002/anie.201402402.

[100] X. Min, J. Xiao, M. Fang, W. Wang, Y. Zhao, Y. Liu, A.M. Abdelkader, K. Xi, R.V. Kumar, Z. Huang, Potassium-ion batteries: outlook on present and future technologies, Energy & Environmental Science 14(4) (2021) 2186-2243. https://doi.org/10.1039/d0ee02917c.

[101] D. Chen, Z. Huang, S. Sun, H. Zhang, W. Wang, G. Yu, J. Chen, A Flexible Multi-Channel Hollow CNT/Carbon Nanofiber Composites with S/N Co-Doping for Sodium/Potassium Ion Energy Storage, ACS Applied Materials & Interfaces (2021) 44369-44378. https://doi.org/10.1021/acsami.1c12470.

[102] K. Sakaushi, E. Hosono, G. Nickerl, T. Gemming, H. Zhou, S. Kaskel, J. Eckert, Aromatic Poreous-Honeycomb Electrodes for A Sodium-organic Energy Storage Device, Nature Communications 4 (2013) 1485. https://doi.org/10.1038/ncomms2481.

[103] H. Xie, Z. Wu, Z. Wang, N. Qin, Y. Li, Y. Cao, Z. Lu, Solid electrolyte interface stabilization via surface oxygen species functionalization in hard carbon for superior performance sodium-ion batteries, Journal of Materials Chemistry A 8(7) (2020) 3606-3612. https://doi.org/10.1039/c9ta12429b.

[104] R.A. Adams, J.-M. Syu, Y. Zhao, C.-T. Lo, A. Varma, V.G. Pol, Binder-Free N- and O-Rich Carbon Nanofiber Anodes for Long Cycle Life K-Ion Batteries, ACS Applied Materials & Interfaces 9(21) (2017) 17872-17881. https://doi.org/10.1021/acsami.7b02476.

[105] Y.-l. Zhong, W.-x. Dai, D. Liu, W. Wang, L.-t. Wang, J.-P. Xie, R. Li, Q.-l. Yuan, G. Hong, Nitrogen and Fluorine Dual Doping of Soft Carbon Nanofibers as Advanced Anode for Potassium Ion Batteries, Small (2021) 2101576. https://doi.org/10.1002/smll.202101576.

[106] C. Lu, Z. Sun, L. Yu, X. Lian, Y. Yi, J. Li, Z. Liu, S. Dou, J. Sun, Enhanced Kinetics Harvested in Heteroatom Dual-Doped Graphitic Hollow Architectures toward High Rate Printable Potassium-Ion Batteries, Advanced Energy Materials 10(28) (2020) 2001161. https://doi.org/10.1002/aenm.202001161.

[107] D. Chao, B. Ouyang, P. Liang, H. Tran Thi Thu, G. Jia, H. Huang, X. Xia, R.S. Rawat, H.J. Fan, C-Plasma of Hierarchical Graphene Survives SnS Bundles for Ultrastable and High Volumetric Na-Ion Storage, Advanced Materials 30(49) (2018) 1804833. https://doi.org/10.1002/adma.201804833.

[108] Y. Lu, P. Zhou, K. Lei, Q. Zhao, Z. Tao, J. Chen, Selenium Phosphide (Se_4P_4) as a New and Promising Anode Material for Sodium-Ion Batteries, Advanced Energy Materials 7(7) (2017) 1601973. https://doi.org/10.1002/aenm.201601973.

[109] D. Chao, C. Zhu, P. Yang, X. Xia, J. Liu, J. Wang, X. Fan, S.V. Savilov, J. Lin, H.J. Fan, Z.X. Shen, Array of nanosheets render ultrafast and high-capacity Na-ion storage by tunable pseudocapacitance, Nature Communications 7 (2016) 1-8. https://doi.org/10.1038/ncomms12122.

[110] W. Zhang, J. Mao, S. Li, Z. Chen, Z. Guo, Phosphorus-Based Alloy Materials for Advanced Potassium-Ion Battery Anode, Journal of the American Chemical Society 139(9) (2017) 3316-3319. https://doi.org/10.1021/jacs.6b12185.

[111] C. Lin, L. Ouyang, C. Zhou, R. Hu, L. Yang, X. Yang, H. Shao, M. Zhu, A novel selenium-phosphorous amorphous composite by plasma assisted ball milling for high-performance rechargeable potassium-ion battery anode, Journal of Power Sources 443 (2019) 227276. https://doi.org/10.1016/j.jpowsour.2019.227276.

[112] J. Chen, L.N. Xu, W.Y. Li, X.L. Gou, alpha-Fe_2O_3 nanotubes in gas sensor and lithium-ion battery applications, Advanced Materials 17(5) (2005) 582-586. https://doi.org/10.1002/adma.200401101.

[113] Q. Zhu, N. Chen, F. Tao, Q. Pan, Improving the lithium storage properties of Fe_2O_3@C nanoparticles by superoleophilic and superhydrophobic polysiloxane coatings, Journal of Materials Chemistry 22(31) (2012) 15894-15900. https://doi.org/10.1039/c2jm31915b.

[114] C. Zhao, X. Shao, Y. Zhang, X. Qian, Fe_2O_3/Reduced Graphene Oxide/Fe_3O_4 Composite in Situ Grown on Fe Foil for High-Performance Supercapacitors, ACS Applied Materials & Interfaces 8(44) (2016) 30133-30142. https://doi.org/10.1021/acsami.6b09594.

[115] Q. Wang, Y. Ma, L. Liu, S. Yao, W. Wu, Z. Wang, P. Lv, J. Zheng, K. Yu, W. Wei, K. Ostrikov, Plasma Enabled Fe_2O_3/Fe_3O_4 Nano-aggregates Anchored on Nitrogen-doped Graphene as Anode for Sodium-Ion Batteries, Nanomaterials 10(4) (2020) 782. https://doi.org/10.3390/nano10040782.

[116] Y. Guo, Z. Yao, C. Shang, E. Wang, P doped Co_2Mo_3Se nanosheets grown on carbon fiber cloth as an efficient hybrid catalyst for hydrogen evolution, Journal of Materials Chemistry A 5(24) (2017) 12043-12047. https://doi.org/10.1039/c7ta03305b.

[117] K. Zhang, M. Park, L. Zhou, G.-H. Lee, W. Li, Y.-M. Kang, J. Chen, Urchin-Like $CoSe_2$ as a High-Performance Anode Material for Sodium-Ion Batteries, Advanced Functional Materials 26(37) (2016) 6728-6735. https://doi.org/10.1002/adfm.201602608.

[118] S. Zhu, Q. Li, Q. Wei, R. Sun, X. Liu, Q. An, L. Mai, $NiSe_2$ Nanooctahedra as an Anode Material for High-Rate and Long-Life Sodium-Ion Battery, ACS Applied Materials & Interfaces 9(1) (2017) 311-316. https://doi.org/10.1021/acsami.6b10143.

[119] S. Zhang, Y. Ai, S.-C. Wu, H.-J. Liao, T.-Y. Su, J.-H. Chen, C.-H. Wang, L. Lee, Y.-Z. Chen, B. Xu, S.-Y. Tang, D.C. Wu, S.-S. Lee, J. Yin, J. Li, J. Kang, Y.-L. Chueh, 3D $CoMoSe_4$ Nanosheet Arrays Converted Directly from Hydrothermally Processed $CoMoO_4$ Nanosheet Arrays by Plasma-Assisted Selenization Process Toward Excellent Anode Material in Sodium-Ion Battery, Nanoscale Research Letters 14 (2019) 213. https://doi.org/10.1186/s11671-019-3035-6.

[120] Q. Gan, H. He, K. Zhao, Z. He, S. Liu, S. Yang, Plasma-Induced Oxygen Vacancies in Urchin-Like Anatase Titania Coated by Carbon for Excellent Sodium-Ion Battery Anodes, ACS Applied Materials & Interfaces 10(8) (2018) 7031-7042. https://doi.org/10.1021/acsami.7b13760.

[121] Q. Zhang, Y. Guo, K. Guo, T. Zhai, H. Li, Ultrafine potassium titanate nanowires: a new Ti-based anode for sodium ion batteries, Chemical Communications 52(37) (2016) 6229-6232. https://doi.org/10.1039/c6cc01057a.

[122] A. Rudola, K. Saravanan, S. Devaraj, H. Gong, P. Balaya, $Na_2Ti_6O_{13}$: a potential anode for grid-storage sodium-ion batteries, Chemical Communications 49(67) (2013) 7451-7453. https://doi.org/10.1039/c3cc44381g.

[123] Z. Yang, J. Sun, Y. Xie, P. Kaur, J. Hernandez, Y. Ni, Y. Yu, O.K. Varghese, Y. Huang, S. Chen, Hydrogen plasma reduced potassium titanate as a high power and ultralong lifespan anode material for sodium-ion batteries, Journal of Materials Chemistry A 6(44) (2018) 22037-22042. https://doi.org/10.1039/c8ta02523a.

[124] C. Yang, Z. Wang, T. Lin, H. Yin, X. Lu, D. Wan, T. Xu, C. Zheng, J. Lin, F. Huang, X. Xie, M. Jiang, Core-Shell Nanostructured "Black" Rutile Titania as Excellent Catalyst for Hydrogen Production Enhanced by Sulfur Doping, Journal of the American Chemical Society 135(47) (2013) 17831-17838. https://doi.org/10.1021/ja4076748.

[125] T. Lin, C. Yang, Z. Wang, H. Yin, X. Lu, F. Huang, J. Lin, X. Xie, M. Jiang, Effective nonmetal incorporation in black titania with enhanced solar energy utilization, Energy & Environmental Science 7(3) (2014) 967-972. https://doi.org/10.1039/c3ee42708k.

[126] Q. Wang, H. He, J. Luan, Y. Tang, D. Huang, Z. Peng, H. Wang, Synergistic effect of N-doping and rich oxygen vacancies induced by nitrogen plasma endows TiO_2 superior sodium storage performance, Electrochimica Acta 309 (2019) 242-252. https://doi.org/10.1016/j.electacta.2019.04.051.

[127] H. He, D. Huang, W. Pang, D. Sun, Q. Wang, Y. Tang, X. Ji, Z. Guo, H. Wang, Plasma-Induced Amorphous Shell and Deep Cation-Site S Doping Endow TiO_2 with Extraordinary Sodium Storage Performance, Advanced Materials 30(26) (2018) 1801013. https://doi.org/10.1002/adma.201801013.

[128] J. Cai, R. Cai, Z. Sun, X. Wang, N. Wei, F. Xu, Y. Shao, P. Gao, S. Dou, J. Sun, Confining TiO_2 Nanotubes in PECVD-Enabled Graphene Capsules Toward Ultrafast K-Ion Storage: In Situ TEM/XRD Study and DFT Analysis, Nano-Micro Letters 12(1) (2020) 123. https://doi.org/10.1007/s40820-020-00460-y.

[129] J. Yang, H. Wang, P. Hu, J. Qi, L. Guo, L. Wang, A High-Rate and Ultralong-Life Sodium-Ion Battery Based on $NaTi_2(PO_4)_3$ Nanocubes with Synergistic Coating of Carbon and Rutile TiO_2, Small 11(31) (2015) 3744-3749. https://doi.org/10.1002/smll.201500144.

[130] Q. Hu, M. Yu, J. Liao, Z. Wen, C. Chen, Porous carbon-coated $NaTi_2(PO_4)_3$with superior rate and low-temperature properties, Journal of Materials Chemistry A 6(5) (2018) 2365-2370. https://doi.org/10.1039/c7ta10207k.

[131] Y. Kong, J. Sun, L. Gai, X. Ma, J. Zhou, $NaTi_2(PO_4)_3$/C||$LiMn_2O_4$ rechargeable battery operating with Li^+/Na^+-mixed aqueous electrolyte exhibits superior electrochemical performance, Electrochimica Acta 255 (2017) 220-229. https://doi.org/10.1016/j.electacta.2017.10.006.

[132] Z.-Y. Wang, R. Zheng, W.-J. Li, Y.-J. Ma, K.-H. Yu, P. Lv, W. Wei, Plasma assisted fabrication of a $NaTi_2(PO_4)_3$@Gr nanocomposite for high-rate and long cycle-life sodium-ion batteries, Sustainable Energy & Fuels 4(9) (2020) 4581-4588. https://doi.org/10.1039/d0se00347f.

[133] X. Zhu, H. Zhang, Z. Wang, C. Zhang, L. Qin, D. Chen, S. Sun, C. Liu, J. Chen, A self-optimized dual zinc/copper-electrolyte anodic interfaces by mechanical rolling toward zinc ion batteries with high capacity and long cycle life, Materials Today Energy 23 (2022) 100897.

[134] W. Luo, C.F. Lin, O. Zhao, M. Noked, Y. Zhang, G.W. Rubloff, L. Hu, Ultrathin surface coating enables the stable sodium metal anode, Advanced Energy Materials 7(2) (2017) 1601526.

[135] R.E.A. Ardhi, G. Liu, J.K. Lee, Metal–Semiconductor Ohmic and Schottky Contact Interfaces for Stable Li-Metal Electrodes, ACS Energy Letters 6(4) (2021) 1432-1442.

[136] P. Liu, D. Mitlin, Emerging Potassium Metal Anodes: Perspectives on Control of the Electrochemical Interfaces, Accounts of Chemical Research 53(6) (2020) 1161-1175. https://doi.org/10.1021/acs.accounts.0c00099.

[137] L. Fan, S. Wei, S. Li, Q. Li, Y. Lu, Recent progress of the solid‐state electrolytes for high‐energy metal‐based batteries, Advanced Energy Materials 8(11) (2018) 1702657.

[138] A. Hagopian, M.-L. Doublet, J.-S. Filhol, Thermodynamic origin of dendrite growth in metal anode batteries, Energy & Environmental Science 13(12) (2020) 5186-5197. https://doi.org/10.1039/d0ee02665d.

[139] H. Jia, M. Qiu, C. Lan, H. Liu, M. Dirican, S. Fu, X. Zhang, Advanced Zinc Anode with Nitrogen-Doping Interface Induced by Plasma Surface Treatment, Advanced Science 9(3) (2022) 2103952. https://doi.org/10.1002/advs.202103952.

[140] M. Zhou, S. Guo, J. Li, X. Luo, Z. Liu, T. Zhang, X. Cao, M. Long, B. Lu, A. Pan, G. Fang, J. Zhou, S. Liang, Surface-Preferred Crystal Plane for a Stable and Reversible Zinc Anode, Advanced Materials 33(21) (2021) 2100187. https://doi.org/10.1002/adma.202100187.

[141] H. Lu, Q. Jin, X. Jiang, D. Zhi-Min, D. Zhang, Y. Jin, Vertical Crystal Plane Matching between $AgZn_3$ (002) and Zn (002) Achieving a Dendrite-Free Zinc Anode, Small (2022) 2200131. https://doi.org/10.1002/smll.202200131.

[142] B. Zhao, J. Li, M. Guillaume, J. Dendooven, C. Detavernier, In vacuo XPS investigation of surface engineering for lithium metal anodes with plasma treatment, Journal of Energy Chemistry 66 (2022) 295-305. https://doi.org/10.1016/j.jechem.2021.08.032.

[143] Z. Wang, Y. Tan, Y. Yang, X. Zhao, Y. Liu, L. Niu, B. Tichnell, L. Kong, L. Kang, Z. Liu, F. Ran, Pomelo peels-derived porous activated carbon microsheets dual-doped with nitrogen and phosphorus for high performance electrochemical capacitors, Journal of Power Sources 378 (2018) 499-510. https://doi.org/10.1016/j.jpowsour.2017.12.076.

[144] Z. Wang, Y. Tan, Y. Liu, L. Niu, L. Kong, L. Kang, F. Ran, New Amphiphilic Block Copolymer-modified Electrodes for Supercapacitors, New Journal of Chemistry 42(2) (2018) 1290-1299. https://doi.org/10.1039/c7nj03427j.

[145] Y. Tan, Y. Liu, L. Kong, L. Kang, F. Ran, Supercapacitor electrode of nano-Co_3O_4 decorated with gold nanoparticles via in-situ reduction method, Journal of Power Sources 363 (2017) 1-8. https://doi.org/10.1016/j.jpowsour.2017.07.054.

[146] Y. Liu, L. Liu, L. Kang, F. Ran, Energy Storage Mechanism of Vanadium Nitride via Intercalating Different Atomic Radius for Expanding Interplanar Spacing, Energy & Environmental Materials (0) (2021) 1-7. https://doi.org/10.1002/eem2.12188.

[147] T. He, Q. Zhao, Q. Wu, J. Zhang, F. Ran, Surfactant induced self-assembly to prepare a vanadium nitride/N, S co-doped carbon high-capacitance anode material, Chemical Communications 57(79) (2021) 10246-10249.

[148] F. Ran, Y. Tan, W. Dong, Z. Liu, L. Kong, L. Kang, In situ polymerization and reduction to fabricate gold nanoparticle-incorporated polyaniline as supercapacitor electrode materials, Polymers for Advanced Technologies 29(6) (2018) 1697-1705. https://doi.org/10.1002/pat.4273.

[149] Y. Tan, Y. Liu, Y. Zhang, C. Xu, L. Kong, L. Kang, F. Ran, Dulse-derived porous carbon-polyaniline nanocomposite electrode for high-performance supercapacitors, Journal of Applied Polymer Science 135(5) (2018) 45776. https://doi.org/10.1002/app.45776.

[150] W. He, R. Li, S. Luo, Progress in Plasma Surface Treatment on Carbon Fiber for Composite Material, Surface Technology 49(7) (2020) 76-89.

[151] X. Sun, J. Bao, K. Li, M.D. Argyle, G. Tan, H. Adidharma, K. Zhang, M. Fan, P. Ning, Advance in Using Plasma Technology for Modification or Fabrication of Carbon-Based Materials and Their Applications in Environmental, Material, and Energy Fields, Advanced Functional Materials 31(7) (2021) 2006287. https://doi.org/10.1002/adfm.202006287.

[152] S.A. Evlashin, J.V. Bondareva, T.F. Aslyamov, Y.V. Lyulin, K.I. Maslakov, K.V. Mironovich, M.A.

Tarkhov, H. Ouerdane, Plasma Modification of Carbon Nanowalls Induces Transition from Superhydrophobic to Superhydrophilic, Nanotechnology 32(43) (2021) 435706. https://doi.org/10.1088/1361-6528/ac153f.

[153] Y.-w. Huang, Q.-f. Yu, M. Li, S.-n. Sun, H. Zhao, S.-x. Jin, J. Fan, J.-g. Wang, An Overview of Low-Temperature Plasma Surface Modification of Carbon Materials for Removal of Pollutants from Liquid and Gas Phases, Plasma Processes and Polymers 18(3) (2021) e2000171. https://doi.org/10.1002/ppap.202000171.

[154] H.D.a.S.C. Gallo, Plasma surface activation and functionalisation of carbon-based materials, in: E.P.K.a.D.A.D. Constantinos A. Charitidis (Ed.), Carbon-based Smart Materials, Berlin ; Boston : De Gruyter, 2020, pp. 17-32.

[155] C. Peng, J. Lang, S. Xu, X. Wang, Oxygen-enriched Activated Carbons from Pomelo Peel in High Energy Density Supercapacitors, RSC Advances 4(97) (2014) 54662-54667. https://doi.org/10.1039/c4ra09395j.

[156] R.K. Gupta, M. Dubey, P. Kharel, Z. Gu, Q.H. Fan, Biochar activated by oxygen plasma for supercapacitors, Journal of Power Sources 274 (2015) 1300-1305. https://doi.org/10.1016/j.jpowsour.2014.10.169.

[157] G.G. Soundarya, B. Nalini, K. Ramachandran, P. Balraju, P. Priyanka, Striking Performance of Plasma-synthesized Carbon from Prosopis Juliflora in a Supercapacitor Application, Journal of Physics D-Applied Physics 55(8) (2022) 085501. https://doi.org/10.1088/1361-6463/ac33d8.

[158] S. Kumar, P. Martin, A. Bendavid, J. Bell, K. Ostrikov, Oriented Graphenes from Plasma-Reformed Coconut Oil for Supercapacitor Electrodes, Nanomaterials 9(12) (2019) 1679. https://doi.org/10.3390/nano9121679.

[159] Z. Wang, W. Zhang, Y. Tan, Y. Liu, L. Kong, L. Kang, F. Ran, Electrolyte-Philic Electrode Material with a Functional Polymer Brush, ACS Applied Materials & Interfaces 11(17) (2019) 16087-16095. https://doi.org/10.1021/acsami.9b03054.

[160] Y. Deng, Y. Xie, K. Zou, X. Ji, Review on recent advances in nitrogen-doped carbons: preparations and applications in supercapacitors, Journal of Materials Chemistry A 4(4) (2016) 1144-1173. https://doi.org/10.1039/c5ta08620e.

[161] X. Feng, Y. Bai, M. Liu, Y. Li, H. Yang, X. Wang, C. Wu, Untangling the Respective Effects of Heteroatom-doped Carbon Materials in Batteries, Supercapacitors and the ORR to Design High Performance Materials, Energy & Environmental Science 14(4) (2021) 2036-2089. https://doi.org/10.1039/d1ee00166c.

[162] P.K. Adusei, S. Gbordzoe, S.N. Kanakaraj, Y.-Y. Hsieh, N.T. Alvarez, Y. Fang, K. Johnson, C. McConnell, V. Shanov, Fabrication and study of supercapacitor electrodes based on oxygen plasma functionalized carbon nanotube fibers, Journal of Energy Chemistry 40 (2020) 120-131. https://doi.org/10.1016/j.jechem.2019.03.005.

[163] P. Dulyaseree, V. Yordsri, W. Wongwiriyapan, Effects of microwave and oxygen plasma treatments on capacitive characteristics of supercapacitor based on multiwalled carbon nanotubes, Japanese Journal of Applied Physics 55(2) (2016) 02bd05. https://doi.org/10.7567/jjap.55.02bd05.

[164] G. Sahoo, S.R. Polaki, S. Ghosh, N.G. Krishna, M. Kamruddin, K. Ostrikov, Plasma-tuneable oxygen functionalization of vertical graphenes enhance electrochemical capacitor performance, Energy Storage Materials 14 (2018) 297-305. https://doi.org/10.1016/j.ensm.2018.05.011.

[165] J. Meng, W. Nie, K. Zhang, F. Xu, X. Ding, S. Wang, Y. Qiu, Enhancing Electrochemical Performance of Graphene Fiber-Based Supercapacitors by Plasma Treatment, ACS Applied Materials & Interfaces 10(16) (2018) 13652-13659. https://doi.org/10.1021/acsami.8b04438.

[166] C.-C. Lai, C.-T. Lo, Plasma oxidation of electrospun carbon nanofibers as supercapacitor electrodes, RSC Advances 5(49) (2015) 38868-38872. https://doi.org/10.1039/c5ra04284d.

[167] S.C. Gallo, X. Li, K. Futterer, C.A. Charitidis, H. Dong, Carbon Nanofibers Functionalized with Active Screen Plasma Deposited Metal Nanoparticles for Electrical Energy Storage Devices, ACS Applied Materials & Interfaces 9(27) (2017) 23195-23201. https://doi.org/10.1021/acsami.7b05567.

[168] Z. Li, S. Qi, Y. Liang, Z. Zhang, X. Li, H. Dong, Plasma Surface Functionalization of Carbon Nanofibres with Silver, Palladium and Platinum Nanoparticles for Cost-Effective and High-Performance

Supercapacitors, Micromachines 10(1) (2019) 2. https://doi.org/10.3390/mi10010002.

[169] Y. Song, Z. Zhao, X. Liu, Y. Yang, C. Leng, H. Zhang, J. Yu, L. Sun, X. Wang, J. Qiu, DBD plasma-tuned functionalization of edge-enriched graphene nanoribbons for high performance supercapacitors, Electrochimica Acta 337 (2020) 135741. https://doi.org/10.1016/j.electacta.2020.135741.

[170] F.-H. Kuok, K.-Y. Kan, I.-S. Yu, C.-W. Chen, C.-C. Hsu, I.C. Cheng, J.-Z. Chen, Application of atmospheric-pressure plasma jet processed carbon nanotubes to liquid and quasi-solid-state gel electrolyte supercapacitors, Applied Surface Science 425 (2017) 321-328. https://doi.org/10.1016/j.apsusc.2017.06.286.

[171] A.R. Hsu, H.-H. Chien, C.-Y. Liao, C.-C. Lee, J.-H. Tsai, C.-C. Hsu, I.C. Cheng, J.-Z. Chen, Scan-Mode Atmospheric-Pressure Plasma Jet Processed Reduced Graphene Oxides for Quasi-Solid-State Gel-Electrolyte Supercapacitors, Coatings 8(2) (2018) 52. https://doi.org/10.3390/coatings8020052.

[172] Z. Jing, S. Qi, X. Tao, H. Yu, W. Zhang, Y. Qiao, X. Li, H. Dong, Active-screen Plasma Multi-functionalization of Graphene Oxide for Supercapacitor Application, Journal of Materials Science 56(4) (2021) 3296-3311. https://doi.org/10.1007/s10853-020-05410-y.

[173] G. Ghanashyam, H.K. Jeong, Synthesis of plasma treated nitrogen-doped graphite oxide for supercapacitor applications, Journal of Energy Storage 26 (2019) 100923. https://doi.org/10.1016/j.est.2019.100923.

[174] N.R. Chodankar, S.-H. Ji, D.-H. Kim, Surface Modified Carbon Cloth via Nitrogen Plasma for Supercapacitor Applications, Journal of the Electrochemical Society 165(11) (2018) A2446-A2450. https://doi.org/10.1149/2.0181811jes.

[175] K. Wang, M. Xu, Y. Gu, Z. Gu, J. Liu, Q.H. Fan, Low-temperature plasma exfoliated N-doped graphene for symmetrical electrode supercapacitors, Nano Energy 31 (2017) 486-494. https://doi.org/10.1016/j.nanoen.2016.11.007.

[176] G. Ghanashyam, H.K. Jeong, Synthesis of nitrogen-doped plasma treated carbon nanofiber as an efficient electrode for symmetric supercapacitor, Journal of Energy Storage 33 (2021) 102150. https://doi.org/10.1016/j.est.2020.102150.

[177] Y. Li, G. Wang, T. Wei, Z. Fan, P. Yan, Nitrogen and sulfur co-doped porous carbon nanosheets derived from willow catkin for supercapacitors, Nano Energy 19 (2016) 165-175. https://doi.org/10.1016/j.nanoen.2015.10.038.

[178] N. Parveen, M.O. Ansari, S.A. Ansari, M.H. Cho, Simultaneous sulfur doping and exfoliation of graphene from graphite using an electrochemical method for supercapacitor electrode materials, Journal of Materials Chemistry A 4(1) (2016) 233-240. https://doi.org/10.1039/c5ta07963b.

[179] X. Wang, Y. Liu, P. Wu, Water-soluble triphenylphosphine-derived microgel as the template towards in-situ nitrogen, phosphorus co-doped mesoporous graphene framework for supercapacitor and electrocatalytic oxygen reduction, Chemical Engineering Journal 328 (2017) 417-427. https://doi.org/10.1016/j.cej.2017.07.064.

[180] T. Zhu, S. Li, B. Ren, L. Zhang, L. Dong, L. Tan, Plasma-induced synthesis of boron and nitrogen co-doped reduced graphene oxide for super-capacitors, Journal of Materials Science 54(13) (2019) 9632-9642. https://doi.org/10.1007/s10853-019-03552-2.

[181] Y. Miao, Y. Ma, Q. Wang, Plasma-Assisted Simultaneous Reduction and Nitrogen/Sulfur Codoping of Graphene Oxide for High-Performance Supercapacitors, ACS Sustainable Chemistry & Engineering 7(8) (2019) 7597-7608. https://doi.org/10.1021/acssuschemeng.8b05838.

[182] Y. Lu, J. Liang, S. Deng, Q. He, S. Deng, Y. Hu, D. Wang, Hypercrosslinked Polymers Enabled Micropore-dominant N, S Co-Doped Porous Carbon for Ultrafast Electron/Ion Transport Supercapacitors, Nano Energy 65 (2019) 103993. https://doi.org/10.1016/j.nanoen.2019.103993.

[183] H. Xu, J. Chen, D. Wang, Z. Sun, P. Zhang, Y. Zhang, X. Guo, Hierarchically Porous Carbon-coated SnO_2@graphene Foams as Anodes for Lithium Ion Storage, Carbon 124 (2017) 565-575. https://doi.org/10.1016/j.carbon.2017.09.016.

[184] C.-H. Yang, F.-H. Kuok, C.-Y. Liao, T.-H. Wan, C.-W. Chen, C.-C. Hsu, I.C. Cheng, J.-Z. Chen, Flexible reduced graphene oxide supercapacitor fabricated using a nitrogen dc- pulse atmospheric-pressure plasma jet, Materials Research Express 4(2) (2017) 025504. https://doi.org/10.1088/2053-1591/aa5ed5.

[185] V. Augustyn, P. Simon, B. Dunn, Pseudocapacitive oxide materials for high-rate electrochemical energy storage, Energy & Environmental Science 7(5) (2014) 1597-1614. https://doi.org/10.1039/c3ee44164d.

[186] J. Jiang, Y. Li, J. Liu, X. Huang, C. Yuan, X.W. Lou, Recent Advances in Metal Oxide-based Electrode Architecture Design for Electrochemical Energy Storage, Advanced Materials 24(38) (2012) 5166-5180. https://doi.org/10.1002/adma.201202146.

[187] H. Liang, C. Xia, Q. Jiang, A.N. Gandi, U. Schwingenschlogl, H.N. Alshareef, Low temperature synthesis of ternary metal phosphides using plasma for asymmetric supercapacitors, Nano Energy 35 (2017) 331-340. https://doi.org/10.1016/j.nanoen.2017.04.007.

[188] Z. Gao, Z. Wu, S. Zhao, T. Zhang, Q. Wang, Enhanced capacitive property of HfN film electrode by plasma etching for supercapacitors, Materials Letters 235 (2019) 148-152. https://doi.org/10.1016/j.matlet.2018.10.032.

[189] Y. Wang, W. Huo, X. Yuan, Y. Zhang, Composite of Manganese Dioxide and Two-dimensional Materials Applied to Supercapacitors, Acta Physico-Chimica Sinica 36(2) (2020) 1904007. https://doi.org/10.3866/pku.Whxb201904007.

[190] M. Sun, H. Liu, J. Qu, J. Li, Earth-Rich Transition Metal Phosphide for Energy Conversion and Storage, Advanced Energy Materials 6(13) (2016) 1600087. https://doi.org/10.1002/aenm.201600087.

[191] Y. Duan, T. Hu, L. Yang, J. Gao, S. Guo, M. Hou, X. Ye, Facile fabrication of electroactive microporous Co_3O_4 through microwave plasma etching for supercapacitors, Journal of Alloys and Compounds 771 (2019) 156-161. https://doi.org/10.1016/j.jallcom.2018.08.204.

[192] H. Liang, C. Xia, A.-H. Emwas, D.H. Anjum, X. Miao, H.N. Alshareef, Phosphine plasma activation of alpha-Fe_2O_3 for high energy asymmetric supercapacitors, Nano Energy 49 (2018) 155-162. https://doi.org/10.1016/j.nanoen.2018.04.032.

[193] P. Cui, Y. Zhang, Z. Cao, Y. Liu, Z. Sun, S. Cheng, Y. Wu, J. Fu, E. Xie, Plasma-assisted Lattice Oxygen Vacancies Engineering Recipe for High-Performing Supercapacitors in a Model of Birnessite-MnO_2, Chemical Engineering Journal 412 (2021) 128676. https://doi.org/10.1016/j.cej.2021.128676.

[194] A. Chang, C. Zhang, Y. Yu, Y. Yu, B. Zhang, Plasma-Assisted Synthesis of $NiSe_2$ Ultrathin Porous Nanosheets with Selenium Vacancies for Supercapacitor, ACS Applied Materials & Interfaces 10(49) (2018) 41861-41865. https://doi.org/10.1021/acsami.8b16072.

[195] F. Ran, Z. Wang, Y. Yang, Z. Liu, L. Kong, L. Kang, Nano vanadium nitride incorporated onto interconnected porous carbon via the method of surface-initiated electrochemical mediated ATRP and heat-treatment approach for supercapacitors, Electrochimica Acta 258 (2017) 405-413. https://doi.org/10.1016/j.electacta.2017.11.076.

[196] Y. Yang, L. Zhao, K. Shen, Y. Liu, X. Zhao, Y. Wu, Y. Wang, F. Ran, Ultra-small vanadium nitride quantum dots embedded in porous carbon as high performance electrode materials for capacitive energy storage, Journal of Power Sources 333 (2016) 61-71. https://doi.org/10.1016/j.jpowsour.2016.09.151.

[197] K. Huang, K. Bi, C. Liang, S. Lin, R. Zhang, W.J. Wang, H.L. Tang, M. Lei, Novel VN/C nanocomposites as methanol-tolerant oxygen reduction electrocatalyst in alkaline electrolyte, Scientific Reports 5 (2015) 11351. https://doi.org/10.1038/srep11351.

[198] Y. Wu, F. Ran, Vanadium nitride quantum dot/nitrogen-doped microporous carbon nanofibers electrode for high-performance supercapacitors, Journal of Power Sources 344 (2017) 1-10. https://doi.org/10.1016/j.jpowsour.2017.01.095.

[199] Y. Yang, Y. Wang, L. Zhao, Y. Liu, F. Ran, Visualizing Nucleation and Growth Process of Vanadium-Supramolecular Nanoribbons Self-Assembled by Rapid Cooling Method towards High-Capacity Vanadium Nitride Anode Materials, Advanced Energy Materials (2022) 2103158. https://doi.org/10.1002/aenm.202103158.

[200] S.G. Kim, J. Jun, Y.K. Kim, J. Kim, J.S. Lee, J. Jang, Facile Synthesis of Co_3O_4-Incorporated Multichannel Carbon Nanofibers for Electrochemical Applications, ACS Applied Materials & Interfaces 12(18) (2020) 20613-20622. https://doi.org/10.1021/acsami.0c06254.

[201] N.R. Chodankar, S. Selvaraj, S.-H. Ji, Y. Kwon, D.-H. Kim, Interface-Engineered Nickel Cobaltite Nanowires through NiO Atomic Layer Deposition and Nitrogen Plasma for High-Energy, Long-Cycle-Life Foldable All-Solid-State Supercapacitors, Small 15(3) (2019) 1803716.

https://doi.org/10.1002/smll.201803716.

[202] C.-Y. Liao, F.-H. Kuok, C.-W. Chen, C.-C. Hsu, J.-Z. Chen, Flexible quasi-solid-state SnO_2/CNT supercapacitor processed by a dc-pulse nitrogen atmospheric-pressure plasma jet, Journal of Energy Storage 11 (2017) 237-241. https://doi.org/10.1016/j.est.2017.03.007.

[203] C.-H. Xu, P.-Y. Shen, Y.-F. Chiu, P.-W. Yeh, C.-C. Chen, L.-C. Chen, C.-C. Hsu, I.C. Cheng, J.-Z. Chen, Atmospheric pressure plasma jet processed nanoporous Fe_2O_3/CNT composites for supercapacitor application, Journal of Alloys and Compounds 676 (2016) 469-473. https://doi.org/10.1016/j.jallcom.2016.03.185.

[204] W.-M. Chang, C.-C. Wang, C.-Y. Chen, Plasma-Induced Polyaniline Grafted on Carbon Nanotube-embedded Carbon Nanofibers for High-Performance Supercapacitors, Electrochimica Acta 212 (2016) 130-140. https://doi.org/10.1016/j.electacta.2016.06.159.

[205] S. Hussain, E. Kovacevic, R. Amade, J. Berndt, C. Pattyn, A. Dias, C. Boulmer-Leborgne, M.-R. Ammar, E. Bertran-Serra, Plasma synthesis of polyaniline enrobed carbon nanotubes for electrochemical applications, Electrochimica Acta 268 (2018) 218-225. https://doi.org/10.1016/j.electacta.2018.02.112.

[206] Y. Han, P. Chen, Y. Xia, S. Huang, W. Chen, W. Lu, Electrodeposition of polypyrrole on He plasma etched carbon nanotube films for electrodes of flexible all-solid-state supercapacitor, Journal of Solid State Electrochemistry 23(5) (2019) 1553-1562. https://doi.org/10.1007/s10008-019-04242-4.

[207] L. Yang, Z. Shi, W. Yang, Polypyrrole directly bonded to air-plasma activated carbon nanotube as electrode materials for high-performance supercapacitor, Electrochimica Acta 153 (2015) 76-82. https://doi.org/10.1016/j.electacta.2014.11.146.

[208] P. Arora, Z.M. Zhang, Battery separators, Chemical Reviews 104(10) (2004) 4419-4462. https://doi.org/10.1021/cr020738u.

[209] S.S. Zhang, A review on the separators of liquid electrolyte Li-ion batteries, Journal of Power Sources 164(1) (2007) 351-364. https://doi.org/10.1016/j.jpowsour.2006.10.065.

[210] Y.M. Lee, J.W. Kim, N.S. Choi, J.A. Lee, W.H. Seol, J.K. Park, Novel porous separator based on PVdF and PE non-woven matrix for rechargeable lithium batteries, Journal of Power Sources 139(1-2) (2005) 235-241. https://doi.org/10.1016/j.jpowsour.2004.06.055.

[211] J.H. Ahn, H.-J. Shin, S. Abbas, K.-Y. Lee, H.Y. Ha, Plasma-functionalized carbon-layered separators for improved performance of lithium sulfur batteries, Journal of Materials Chemistry A 7(8) (2019) 3772-3782. https://doi.org/10.1039/c8ta10795e.

[212] S.Y. Jin, J. Manuel, X. Zhao, W.H. Park, J.-H. Ahn, Surface-modified polyethylene separator via oxygen plasma treatment for lithium ion battery, Journal of Industrial and Engineering Chemistry 45 (2017) 15-21. https://doi.org/10.1016/j.jiec.2016.08.021.

[213] M. Han, D.-W. Kim, Y.-C. Kim, Charged Polymer-Coated Separators by Atmospheric Plasma Induced Grafting for Lithium-Ion Batteries, ACS Applied Materials & Interfaces 8(39) (2016) 26073-26081. https://doi.org/10.1021/acsami.6b08781.

[214] J. Luan, Q. Zhang, H. Yuan, D. Sun, Z. Peng, Y. Tang, X. Ji, H. Wang, Plasma-Strengthened Lithiophilicity of Copper Oxide Nanosheet-Decorated Cu Foil for Stable Lithium Metal Anode, Advanced Science 6(20) (2019) 1901433. https://doi.org/10.1002/advs.201901433.

[215] J. Zhu, J. Chen, Y. Luo, S. Sun, L. Qin, H. Xu, P. Zhang, W. Zhang, W. Tian, Z. Sun, Lithiophilic metallic nitrides modified nickel foam by plasma for stable lithium metal anode, Energy Storage Materials 23 (2019) 539-546. https://doi.org/10.1016/j.ensm.2019.04.005.

[216] G. Li, Y. Wang, H. Guo, Z. Liu, P. Chen, X. Zheng, J. Sun, H. Chen, J. Zheng, X. Li, Direct plasma phosphorization of Cu foam for Li ion batteries, Journal of Materials Chemistry A 8(33) (2020) 16920-16925. https://doi.org/10.1039/d0ta02512g.